Real-Time Substrate Feed Optimization of Anaerobic Co-Digestion Plants

Gaida, D.

Chapter 9

Dynamic Real-Time Substrate Feed Optimization of a Biogas Plant

9.1 Introduction

In Chapter 2 the MONMPC optimization problem was stated (eqs. (2.20) - (2.22)), whose eqs. are repeated here for convenience:

For each $k = 0, 1, 2, \dots$ set $t_k = k \cdot \delta$ and solve:

$$\begin{aligned} & \mathcal{PF}_k^* := \min_{\underline{\boldsymbol{u}} \in \mathcal{U}_\mathcal{F}} \boldsymbol{J}\left({}^o\boldsymbol{x}(\tau), \underline{\boldsymbol{u}}\right) \\ \text{subject to} \quad & {}^o\boldsymbol{x}'(\tau) = \boldsymbol{f}\left({}^o\boldsymbol{x}(\tau), {}^o\boldsymbol{u}(\tau), \mathbf{0}\right), \qquad {}^o\boldsymbol{x}\left(t_k\right) = \boldsymbol{x}\left(t_k\right), \\ & {}^o\boldsymbol{x}(\tau) \in \mathcal{X}, \qquad \forall \tau \in \left[t_k, t_k + T_\mathrm{p}\right], \\ & {}^o\boldsymbol{u} : \left[t_k, t_k + T_\mathrm{p}\right] \to \boldsymbol{f}_\mathcal{U}\left(\underline{\boldsymbol{u}}\right), \end{aligned} \tag{9.1}$$

with equation (2.21)

$$\underline{\boldsymbol{u}}_k^* := \arg \min_{\forall \underline{\boldsymbol{u}} \in \mathcal{P}_k^*} \sum_{i_\mathrm{o}=1}^{n_\mathrm{o}} \varpi_{i_\mathrm{o}} \cdot J_{\boldsymbol{x}, i_\mathrm{o}}\left(\underline{\boldsymbol{u}}\right) \tag{9.2}$$

and application of equation (2.22)

$$\boldsymbol{u}(t) = {}^o\boldsymbol{u}_k^*(t) = \boldsymbol{f}_\mathcal{U}\left(\underline{\boldsymbol{u}}_k^*\right), \qquad t \in \left[t_k, t_k + \delta\right). \tag{9.3}$$

In this chapter MONMPC is applied to the simulation model of the biogas plant introduced in Section 7.4 in four performance experiments (I - IV), each containing various tests. The same simulation model is used as model $\boldsymbol{f}$ inside the NMPC formulation. To take into account plant-model mismatch, measurement noise and errors is important during evaluation of the control. Therefore, for the controlled simulation model these effects are additionally implemented in some tests, see Section 9.3.2.
As objective function $\boldsymbol{J}$ in eq. (9.1) the one defined in Section 7.3.4 is used. In experiment II and III this objective function is extended by an additional setpoint

control term, which is described in the according sections 9.3.4 and 9.3.5.

In all but the last experiment (IV, Section 9.3.6) the current state vector $\boldsymbol{x}(t_k)$ is directly taken out of the controlled simulation model. Thus, in experiments I to III a perfect state estimator is used. Only in experiment IV a real state estimation algorithm is used. There, some of the previous tests are repeated to see the deterioration of the quality of the results introduced by the state estimator out of Chapter 8.

Each input variable $u_{i_\mathrm{u},i}$, $i_\mathrm{u} = 1, \ldots, n_\mathrm{u}$ and $i = 1, \ldots, s_\mathrm{c}$ (see eq. (2.9)) represents the volumetric flow rate of a substrate, measured in $\frac{\mathrm{m}^3}{\mathrm{d}}$. The i_uth input variable, $i_\mathrm{u} = 1, \ldots, n_\mathrm{u}$, is bound between constant lower $\mathrm{LB}_{i_\mathrm{u}} \in \mathcal{U}_{i_\mathrm{u}}$ and upper $\mathrm{UB}_{i_\mathrm{u}} \in \mathcal{U}_{i_\mathrm{u}}$ boundaries, thus $\mathrm{LB}_{i_\mathrm{u}} \leq u_{i_\mathrm{u},i} \leq \mathrm{UB}_{i_\mathrm{u}}$ or equally $\mathcal{U}_{i_\mathrm{u}} := [\mathrm{LB}_{i_\mathrm{u}}, \mathrm{UB}_{i_\mathrm{u}}]$. In experiment II both boundary vectors $\mathbf{LB} := (\mathrm{LB}_1, \ldots, \mathrm{LB}_{i_\mathrm{u}}, \ldots, \mathrm{LB}_{n_\mathrm{u}})^T \in \mathcal{U}$ and $\mathbf{UB} := (\mathrm{UB}_1, \ldots, \mathrm{UB}_{i_\mathrm{u}}, \ldots, \mathrm{UB}_{n_\mathrm{u}})^T \in \mathcal{U}$ depend on the available dynamically changing feed stock, see Section 9.3.4, in all other experiments they are constant.

9.2 Control Structure

In Figure 9.1 the complete control loop developed in this thesis is shown. It is dedicated to optimally control the substrate feed of anaerobic co-digestion plants. In this section the functionality and structure of the control loop is explained.

As pointed out in the summary of Chapter 2 (Section 2.4) offset-free control using model-based control does not come naturally. In case of plant-model mismatch there can be a steady-state offset because the control error is not directly minimized by the model-based control. To avoid such an offset a cascading control is developed, where the MONMPC is the master and a simpler setpoint control is the slave control. The slave control should track a directly measurable process value. Depending on the application this might be the produced volumetric methane flow rate Q_{ch_4} (for ABP) or the effluent VFA or COD (for anaerobic waste treatment plants), cf. Definitions 6.1 and 6.2 in Chapter 6. Note that online-measurement of effluent COD is expensive but possible using UV/Vis spectroscopy (Langergraber et al., 2004, Brito et al., 2013).

The setpoint (here it is assumed the methane setpoint $Q^*_{\mathrm{ch}_4}(t)$) is set by the master loop containing the MONMPC, which is performing the real-time optimization. As process control a methane setpoint control can be used (e.g. (Hilgert et al., 2000, Antonelli et al., 2003)), which controls the dilution rate $D(t)$. The solution of the MONMPC optimization problem at time t_k is the optimal methane setpoint $Q^*_{\mathrm{ch}_4}(t)$ as well as the corresponding optimal substrate feed ${}^o\boldsymbol{u}^*_k[t_k, t_k + \delta)$. Both are passed to the process control, see Figure 9.1. The process control changes the dilution rate $D(t)$ based on the given control error

$$e_{\mathrm{ch}_4}(t) := Q^*_{\mathrm{ch}_4}(t) - Q_{\mathrm{ch}_4}(t). \tag{9.4}$$

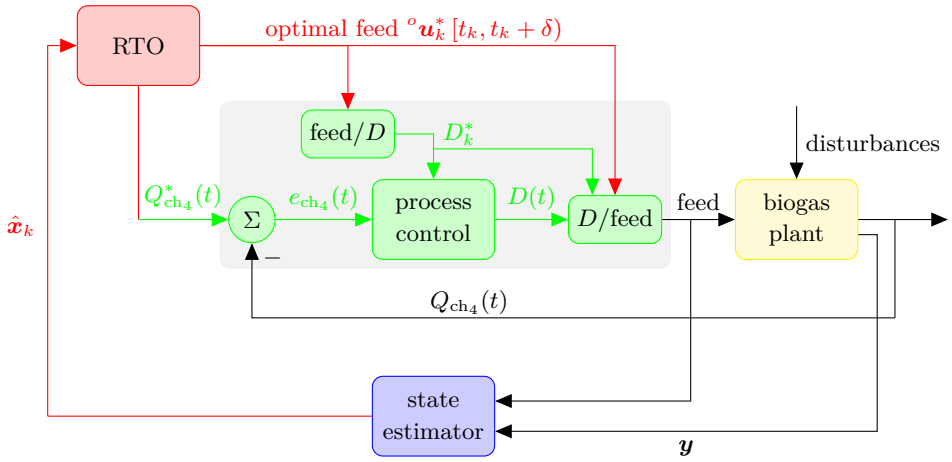

Figure 9.1: Real-Time Substrate Feed Optimization. The background colours of the blocks visualize where they are implemented. The green and yellow blocks are implemented in Simulink® for evaluation purposes. When the control should be applied to the real biogas plant, then the green blocks must be implemented in the PLC (programmable logic controller). The red block is always implemented in MATLAB® and the blue block is implemented in MATLAB® with optional usage of Simulink®.

Here the dilution rate $D(t)$ can be seen as a scaling factor which is only altered by the process control in case of model inaccuracies or process disturbances. The scaling is done in the "D/feed" block in Figure 9.1 where the given optimal substrate feed ${}^{o}\boldsymbol{u}_k^*\,[t_k, t_k+\delta)$ is scaled by $\frac{D(t)}{D_k^*}$, with the optimal dilution rate calculated in the "feed/D" block

$$D_k^* := \frac{\sum_{i_\mathrm{u}=1}^{n_\mathrm{u}} {}^{o}u_{i_\mathrm{u},k}^*\,[t_k, t_k+\delta)}{V_\mathrm{liq}}. \tag{9.5}$$

Then, the feed applied to the biogas plant $\boldsymbol{u}_\mathrm{ctrl}$ is given by:

$$\boldsymbol{u}_\mathrm{ctrl}(t) := {}^{o}\boldsymbol{u}_k^*\,[t_k, t_k+\delta) \cdot \frac{D(t)}{D_k^*}. \tag{9.6}$$

The state estimator in Figure 9.1 is needed so that the dynamic model in the real-time optimization block knows the current state of the biogas plant. In practice the state $\boldsymbol{x}$ is estimated by the state estimator given in Chapter 8. Using this control scheme the given setpoint is robustly controlled and the setpoint itself is set to guarantee stable and optimal control.

This control structure is used in all experiments, with the restriction that in all but the last experiment (Section 9.3.6) a perfect state estimator is used leading to the simplified structure visualized in Figure 9.2.

As process control the very simple approach of Antonelli et al. (2003) is used. It just

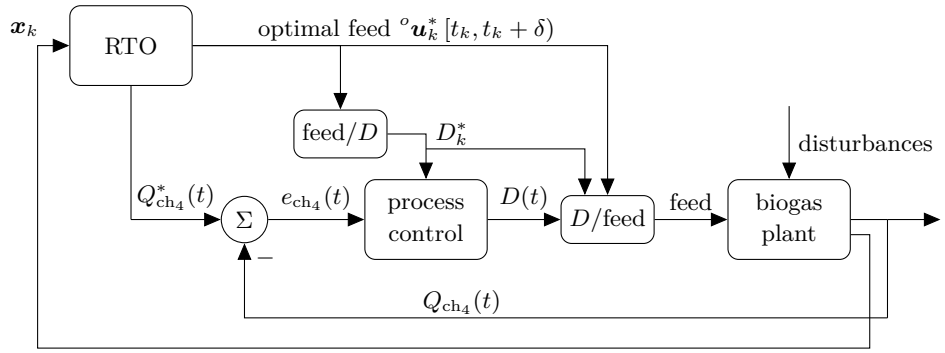

Figure 9.2: Real-Time Substrate Feed Optimization without State Estimator.

consists out of the one equation ($k_{\mathrm{ch_4}} > 0$):

$$D'(t) = k_{\mathrm{ch_4}} \cdot \left(Q_{\mathrm{ch_4}}(t) - Q^*_{\mathrm{ch_4}}(t)\right) \cdot (D(t) - D_{\max,k}) \cdot (D(t) - D_{\min,k}) \tag{9.7}$$

Here, the boundaries $D_{\min,k}$ and $D_{\max,k}$ are set according to ($\Delta D \geq 0\ \frac{1}{\mathrm{d}}$)

$$D_{\min,k} = D_k^* - \Delta D \quad \text{and} \quad D_{\max,k} = D_k^* + \Delta D \tag{9.8}$$

with the optimal dilution rate D_k^* determined by the real-time optimization, see eq. (9.5).

As this control has some limitations, in this thesis an extension is developed as follows. The factor $k_{\mathrm{ch_4}}$ of the original approach in eq. (9.7) is made dependent on the time derivative of the control error $e_{\mathrm{ch_4}}(t)$. In the new approach $k_{\mathrm{ch_4}}$ must be replaced by the term given in equation (9.9), $k_{\mathrm{ch_4}}, k_{\mathrm{ch_4,rel}} > 0$.

$$k_{\mathrm{ch_4}} + k_{\mathrm{ch_4,rel}} \cdot \left[\min\left(e_{\mathrm{ch_4}}(t), 0\right) \cdot \min\left(e'_{\mathrm{ch_4}}(t), 0\right) + \max\left(e_{\mathrm{ch_4}}(t), 0\right) \cdot \max\left(e'_{\mathrm{ch_4}}(t), 0\right)\right] \tag{9.9}$$

Using this extension the original factor $k_{\mathrm{ch_4}}$ is increased if the signs of the control error $e_{\mathrm{ch_4}}(t)$ and its derivative $e'_{\mathrm{ch_4}}(t)$ are the same. Both signs are the same if the control error is negative and decreasing or positive and increasing, respectively. Both situations are not favorable, so that $k_{\mathrm{ch_4}}$ is increased to in-/decrease the dilution rate D faster. On the one hand this is advantageous, but on the other hand using the derivative of the control error $e'_{\mathrm{ch_4}}(t)$ makes the control numerically more difficult. Furthermore, the derivative of the control error in reality can be rather noisy. Unfortunately, using this control in the Simulink® model of the modeled biogas plant did not work out because of numerical problems. Therefore, this control could not yet be tested at the simulation model. Nevertheless, it is planned to use it in the future to control the feed of a pilot-scale biogas plant and compare it with its original control by Antonelli et al. (2003).

9.3 Performance Experiments

In this section the results obtained in the four performance experiments

- Experiment I: Steady-state optimal feed (Section 9.3.3)
- Experiment II: Change of substrate mixture (Section 9.3.4)
- Experiment III: Setpoint control (Section 9.3.5)
- Experiment IV: State estimator (Section 9.3.6)

are presented and discussed. All four performance experiments are performed on three different computers. They are:

- Computer 1 (PC 1): Intel® Core™ i7-4770 CPU @ 3.40 GHz, 16.0 GB RAM, Windows 8, 64 bit
- Computer 2 (PC 2): Intel® Core™ i5-750 CPU @ 2.67 GHz, 4.0 GB RAM, Windows 7, 64 bit
- Computer 3 (PC 3): Intel® Core™2 Quad Q6600 CPU @ 2.40 GHz, 4.0 GB RAM, Windows 7, 64 bit

The obtained results are compared based on the fitness $J_{1\mathrm{D}}$ (7.70), one-dimensional stage cost $F_{1\mathrm{D}}$ (7.71), the hypervolume indicator I_{H} (Def. 3.1), the R2 (9.10) and Δ_{p} (9.13) indicator. The R2 indicator is defined in equation (9.10) (Trautmann et al., 2013).

$$\mathrm{R2} := \frac{1}{\mathrm{card}\,(\mathcal{Q})} \sum_{\boldsymbol{\lambda}\in\mathcal{Q}} \min_{\boldsymbol{\varphi}\in\mathcal{PF}^*} \left\{ \max_{i_\mathrm{o}=1,\ldots,n_\mathrm{o}} \left\{ \lambda_{i_\mathrm{o}} \cdot (\varphi_{i_\mathrm{o}} - i_{i_\mathrm{o}}) \right\} \right\} \tag{9.10}$$

The R2 indicator of the Pareto front $\mathcal{PF}^*$ with elements $\boldsymbol{\varphi} := (\varphi_1, \ldots, \varphi_{n_\mathrm{o}})^T \in \mathcal{PF}^*$ given in eq. (9.10) depends on the ideal point $\mathbf{i} := (i_1, \ldots, i_{n_\mathrm{o}})^T \in \mathbb{R}^{n_\mathrm{o}}$ and weight vectors $\boldsymbol{\lambda} := (\lambda_1, \ldots, \lambda_{n_\mathrm{o}})^T \in \mathcal{Q}$ taken out of the set of weight vectors $\mathcal{Q} \subset \mathbb{R}^{n_\mathrm{o}}$. In total 512 weight vectors $\boldsymbol{\lambda}$, $\|\boldsymbol{\lambda}\|_1 = 1$, are drawn from a normal distribution with mean 0.5 and standard deviation 0.2, bound between 0 and 1 and then each component λ_{i_o} is scaled by the corresponding weight ϖ_{i_o} (see eq. (2.19)). The normal distribution is favored over the uniform one, to concentrate more on the central points in the Pareto front that are much more likely to be chosen by the decision maker. The weights ϖ_{i_o} are set to $\varpi_1 = 0.125$ and $\varpi_2 = 1$.

The Δ_{p} indicator of an approximation set $\mathcal{A} \in \mathbb{R}^{n_\mathrm{o}}$ for the Pareto front $\mathcal{PF}^*$ is defined as in Schütze et al. (2012) using slightly modified versions of the generational distance GD_{p} (9.11) and inverted generational distance $\mathrm{IGD}_{\mathrm{p}}$ (9.12) indicators, $\mathrm{p} \in \mathbb{N}$.

$$\mathrm{GD}_{\mathrm{p}}\,(\mathcal{A}) := \left(\frac{1}{\mathrm{card}\,(\mathcal{A})} \cdot \sum_{\boldsymbol{a}_\mathcal{A}\in\mathcal{A}} \left(\inf_{\boldsymbol{\varphi}\in\mathcal{PF}^*} \|\boldsymbol{a}_\mathcal{A} - \boldsymbol{\varphi}\|_2 \right)^{\mathrm{p}} \right)^{\frac{1}{\mathrm{p}}} \tag{9.11}$$

$$\mathrm{IGD_p}\left(\mathcal{A}\right) := \left(\frac{1}{\mathrm{card}\left(\mathcal{PF}^*\right)} \cdot \sum_{\boldsymbol{\varphi} \in \mathcal{PF}^*} \left(\inf_{\boldsymbol{a}_\mathcal{A} \in \mathcal{A}} \left\| \boldsymbol{a}_\mathcal{A} - \boldsymbol{\varphi} \right\|_2 \right)^\mathrm{p} \right)^{\frac{1}{\mathrm{p}}} \tag{9.12}$$

The Δ_p indicator is then given in eq. (9.13) (Schütze et al., 2012).

$$\Delta_\mathrm{p}\left(\mathcal{A}\right) := \max\left(\mathrm{GD_p}, \mathrm{IGD_p}\right) \tag{9.13}$$

Here, $\mathrm{p} = 1$ is selected, thus Δ_1 of the set $\mathcal{A}$ is calculated. As the true Pareto front $\mathcal{PF}^*$ often is not known, the Δ_p indicator must often be calculated against an optimal Pareto front approximation. Here, the one visualized in Figure 9.5 is used, see Section 9.3.3.2.

9.3.1 Implementation of Optimization Methods

To solve the minimization problem in eq. (9.1) three different optimization methods are evaluated in these experiments. The one most often used is the multi-objective method SMS-EGO. It is compared against the methods SMS-EMOA (see Section 3.1.1) and CMA-ES (Hansen, 2006). All algorithms are implemented in MATLAB®. The latter two methods (SMS-EMOA by Fabian Kretzschmar and Tobias Wagner and CMA-ES by Nikolaus Hansen) are freely available for download[1,2], whereas Tobias Wagner is greatly acknowledged for giving me the opportunity to use his MATLAB® implementation of SMS-EGO.

Both multi-objective optimization methods are configured (changed) so that they use the Pareto optimal set of the previous run at time t_{k-1} as initial points of the current run k. More precisely, for SMS-EMOA the complete previous population is used as initial population (not only the Pareto optimal set). For SMS-EGO at least five by Latin hypercube sampling (LHS) (Jin et al., 2005) selected individuals are used, the remaining initial points are taken out of the previous population starting with the Pareto optimal individuals. Furthermore, the optimal parameters of the previous DACE model are used as initial parameters for the DACE model used in the next run.

In the used CMA-ES implementation the previous population can not be used directly as initial population. Here, the best ever solution from the previous run $k-1$ is used to calculate the new population for the kth run.

9.3.1.1 Choice of Optimization Methods

The chosen optimization algorithms are all derivative-free and global methods. The question is why these methods are chosen and whether also algorithms could be chosen that do not possess these two properties.

[1] http://ls11-www.cs.uni-dortmund.de/rudolph/hypervolume/start
[2] https://www.lri.fr/~hansen/cmaes_inmatlab.html

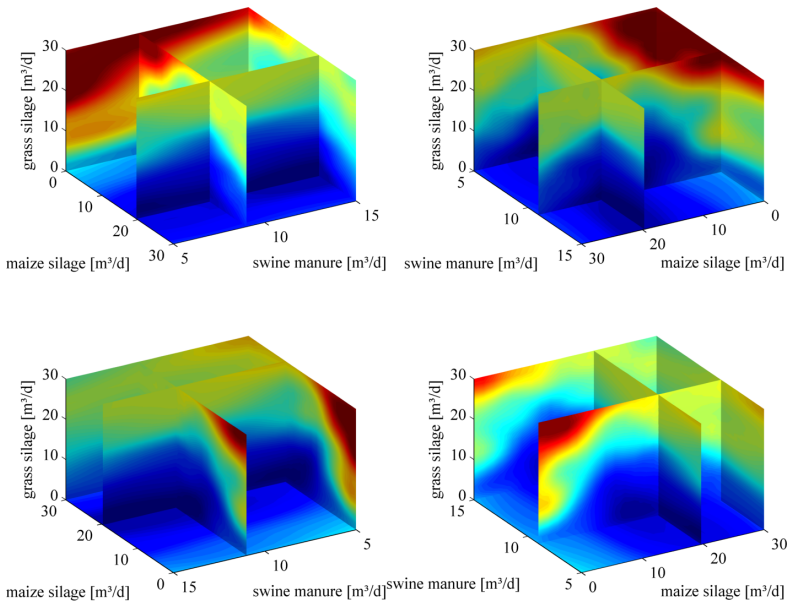

Figure 9.3: Landscape of one-dimensional steady-state stage cost F_{1D}. Each plot is created out of data taken from 1040 simulations, each simulation ran with a constant substrate feed taken from an equidistant distributed grid of substrate feeds. The interpolation of the data points is performed using a Kriging model.

As the objective function used here is quite complex, to determine the gradient of it with respect to the optimization variables analytically would be very difficult or even impossible. As the objective function contains some hard constraints it will not be possible to find a derivative for all components of the objective function. Therefore, derivative-free algorithms have a clear advantage here, because they do not need to know the gradient of the objective function.

Global optimization methods are used when the objective function possesses a lot of local optima. As local optimization algorithms easily get stuck in such local minima they are not suited for that kind of optimization problems. To get an idea whether the objective function used here has local optima the one-dimensional steady-state stage cost F_{1D} is plotted over the three substrates, which are used later during optimization. The results are depicted in Figure 9.3. It can be seen that the landscape is quite nonlinear but here there are not that many local minima. Therefore, it might be possible to also use derivative-free local optimization methods and obtain good results. An example could be to use the downhill simplex method by Nelder and Mead (1965). Therefore, as fourth optimization method MATLAB®'s fminsearchbnd algorithm is used that implements the simplex method of Lagarias et al. (1998).

Table 9.1: Miscalibrated values of substrate dependent ADM1 parameters to emulate plant-model mismatch. To be compared with Table 7.7, whose values are given here in brackets.

Substrate	k_{dis}	$k_{\mathrm{m,c4}}$	$k_{\mathrm{m,pro}}$	$k_{\mathrm{m,ac}}$	$k_{\mathrm{m,h2}}$
maize silage	0.1 (0.14)	20 (20)	4.0 (3.8)	5.0 (4.8)	35.0 (35.9)
swine manure	0.25 (0.27)	20 (20)	3.6 (3.8)	7.0 (6.8)	36.9 (36.1)
grass silage	0.09 (0.04)	20 (20)	7.7 (8)	4.6 (4.9)	36.1 (35.6)

9.3.2 Real World Simulation

To make the experiments as realistic as possible in some tests the model to be controlled is changed a little bit. In total, three changes are applied. First, to account for plant-model mismatch the ADM1 parameters calibrated in Section 7.5 are set to slightly different values, see Table 9.1. As second change the three parameters $\mathrm{TS_{IN}}, \mathrm{VS_{IN}}$ and $\mathrm{pH_{IN}}$ of the substrates are made noisy as can be seen in Figure 9.4. Last, noise and drift are added to some measured variables, see the following list, using the sensor implementation of Rieger et al. (2003).

- sensor Q_{gas}: noise $\mathcal{N}\left(0\ \frac{\mathrm{m}^3}{\mathrm{d}}, 32.5\ \frac{\mathrm{m}^3}{\mathrm{d}}\right)$, drift of 0.5 $\frac{\mathrm{m}^3}{\mathrm{d}}$, re-calibration after each 365 d
- sensor $r_{\mathrm{ch_4}}$: noise $\mathcal{N}\left(0\ \%, 0.5\ \%\right)$, drift of 0.05 %, re-calibration after each 31 d
- sensor $r_{\mathrm{co_2}}$: noise $\mathcal{N}\left(0\ \%, 0.5\ \%\right)$, drift of 0.05 %, re-calibration after each 31 d
- sensor pH: noise $\mathcal{N}\left(0, 0.07\right)$, drift of 0.01, re-calibration after each 14 d
- sensor Q_{IN}: noise $\mathcal{N}\left(0\ \frac{\mathrm{m}^3}{\mathrm{d}}, 0.25\ \frac{\mathrm{m}^3}{\mathrm{d}}\right)$, drift of 0.0 $\frac{\mathrm{m}^3}{\mathrm{d}}$, re-calibration after each 365 d

Using these changes it is expected to create more realistic tests, so that the controller is optimally prepared for real world applications. Further realism could be added as in (Rosen et al., 2008). A process disturbance caused by fluctuations in the digester temperature is not modeled. The reason is that the stoichiometry of the implemented ADM1 is not temperature dependent yet. For a temperature dependent AD model see (Donoso-Bravo et al., 2013).

9.3.3 Experiment I: Steady-State Optimal Feed

In the first set of tests the biogas plant is in a stationary environment. The task is to find the optimal substrate feed for a steady-state operation which in the long run has the best performance. Therefore, in experiment I the following questions are tackled in different simulation studies:

1. Does MONMPC find the true Pareto front of the stage cost $\boldsymbol{F}$ at steady state?
2. How large is the basin of attraction of the found Pareto front?
3. Is the closed loop control stable?
4. Can the results be repeated?

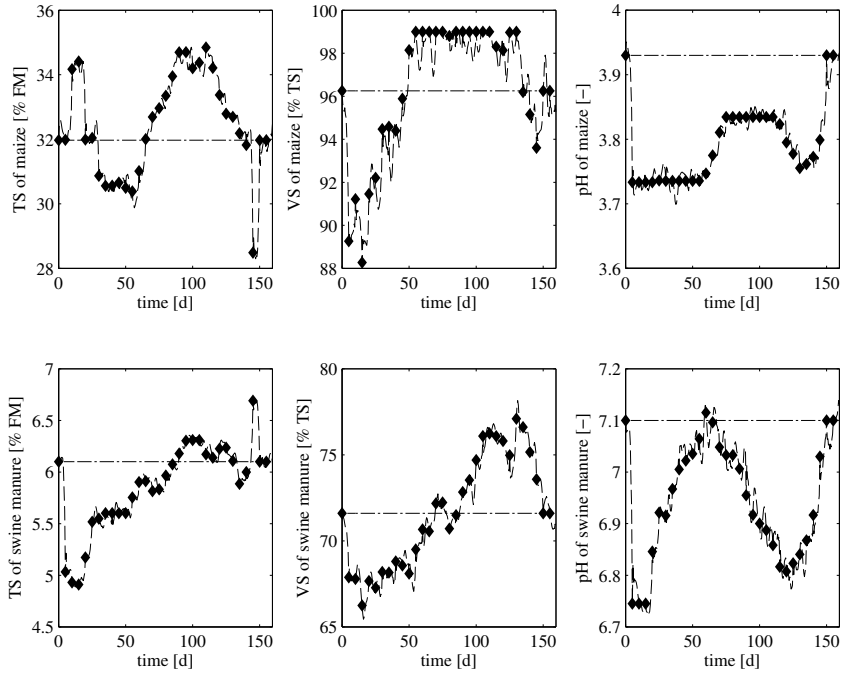

Figure 9.4: Noisy parameters $\mathrm{TS_{IN}}, \mathrm{VS_{IN}}$ and $\mathrm{pH_{IN}}$ of the substrates maize silage and swine manure. The horizontal dash-dotted line in each plot visualizes the nominal value of the parameter used in the ideal world simulations. The diamonds show when offline analysis were done of the parameters, which is in a five day interval. The dashed, noisy curve shows the online measured values. The noise is drawn from a zero-mean normal distribution with 2 % error amplitude for $\mathrm{TS_{IN}}$ and $\mathrm{VS_{IN}}$ and 1 % for $\mathrm{pH_{IN}}$.

9.3.3.1 Setup

Using simulation these questions cannot be answered conclusively. By designing well suited tests the questions can only be answered for the obtained results.

The first question is particularly difficult to answer. In the following the Pareto front of the stage cost $\boldsymbol{F}$ at steady state is called steady-state Pareto front. Here, we search for the Pareto front of the stage cost $\boldsymbol{F}$ and not of the objective function $\boldsymbol{J}$ because we are only interested in the performance of a steady-state operation and not in the costs needed to get there. To determine the steady-state Pareto front, the only possible approach seems to be to compare the results obtained by the MONMPC with results gained by other multi-objective optimization methods which are applied in an open loop fashion, see eq. (9.14). In the optimization problem $t_{\mathrm{end}} = 750$ d is seen as a long

enough simulation duration so that a steady state is reached.

$$\begin{aligned} & \mathcal{PF}^*_{\boldsymbol{F}} := \min_{\underline{\boldsymbol{u}} \in \mathcal{U}_{\mathcal{F}}} \boldsymbol{F}\left({}^o\boldsymbol{x}\left(t_{\mathrm{end}}\right), \underline{\boldsymbol{u}}\right) \\ \text{subject to} \quad & {}^o\boldsymbol{x}'(\tau) = \boldsymbol{f}\left({}^o\boldsymbol{x}(\tau), {}^o\boldsymbol{u}\left(0\right), \boldsymbol{0}\right), \qquad {}^o\boldsymbol{x}\left(0\right) = \boldsymbol{x}\left(0\right), \\ & {}^o\boldsymbol{x}(\tau) \in \mathcal{X}, \qquad \forall \tau \in [0, t_{\mathrm{end}}], \\ & {}^o\boldsymbol{u} : [0, t_{\mathrm{end}}] \to \boldsymbol{f}_{\mathcal{U}}\left(\underline{\boldsymbol{u}}\right), \qquad s_{\mathrm{c}} = 1. \end{aligned} \tag{9.14}$$

To study the second question the MONMPC is started at four different initial substrate feeds (see Table 9.2) to test whether the steady-state Pareto front is the same for all tests. Based on the obtained steady-state Pareto front, it can be concluded whether the corresponding substrate feed did or did not belong to the basin of attraction of the true steady-state Pareto front.
Stability of the closed loop is once investigated without noise, to test whether the control keeps the feed constant once the optimal steady state was found. This is to test whether the control is stationary. Furthermore, all experiments are repeated with measurement noise, drift and disturbances added to the controlled simulation model to examine the stability of the control towards such disturbances acting on the process.

Table 9.2: Initial substrate feeds and lower/upper boundaries (**LB**, **UB**) for substrates. The feeds of test I.A and I.C are moderate. The one of test I.B is very low and the one of test I.D is very high.

component	Test I.A	Test I.B	Test I.C	Test I.D	**LB**	**UB**	unit
Q_{maize}	15	5	40	85	0	30	m^3/d
Q_{manure}	10	5	30	85	5	15	m^3/d
Q_{grass}	2	0	10	45	0	30	m^3/d

To answer the last question some tests are repeated to get an estimate of the scattering in the results. This also applies to all other experiments performed further below in the other sections 9.3.4 - 9.3.6.
The effect of different parameters and configurations on the answers of above questions is investigated as well. They are:

- Optimization methods: Multi-objective as well as single-objective
- Algorithm parameters: Objective function $\boldsymbol{J}$ evaluations $n_{\mathrm{eval}} \in \mathbb{N}$ and initial population size $n_{\mathrm{pop}} \in \mathbb{N}$
- Control parameters: Control horizon T_{c}, prediction horizon T_{p} and control sampling time δ

To avoid a combinatorial explosion not all parameters are changed at the same time. The parameter sets for all tests in experiment I are given in Table 9.3. All parameter sets are performed once for each initial substrate feed I.A to I.D. Therefore, the ID of a test in experiment I could be I.A5 or I.B2. In the first six tests in Table 9.3 the control

parameters prediction T_p and control horizon T_c are studied. As in experiment I the focus is on the steady-state solution the main emphasis is put here on the prediction horizon T_p (test I.1 until I.5) and only in test I.6 the control horizon T_c is changed. In all tests the control sampling time δ is set to the control horizon T_c, so that the substrate feed is only changed once over the control horizon ($s_\mathrm{c} = 1$, see eq. (2.9)). The MATLAB® implementation in principle allows to choose $s_\mathrm{c} > 1$ but as this increases the complexity of the optimization problem this option is not studied here. For more information about the implementation of this option and performance investigations see the Master's thesis of Venkatesan (2012). In tests I.7 to I.10 the effect of the number of simulations in each iteration n_eval is validated for the method SMS-EGO. In tests I.11 until I.14 and I.15 until I.18 two other optimization methods are evaluated. They are the multi-objective method SMS-EMOA and the single-objective method CMA-ES (see Section 9.3.1). Finally, in tests I.19 to I.21 the simplex method (fminsearchbnd) is used.

Table 9.3: Parameter sets for all tests in experiment I.

test no.	T_p/[d]	T_c/[d]	δ/[d]	n_pop	n_eval	method
1	50	10	10	32	50	SMS-EGO
2	100	10	10	32	50	SMS-EGO
3	150	10	10	32	50	SMS-EGO
4	200	10	10	32	50	SMS-EGO
5	300	10	10	32	50	SMS-EGO
6	200	5	5	32	50	SMS-EGO
7	150	10	10	32	40	SMS-EGO
8	150	10	10	32	60	SMS-EGO
9	200	10	10	32	40	SMS-EGO
10	200	10	10	32	60	SMS-EGO
11	150	10	10	20	60	SMS-EMOA
12	150	10	10	25	75	SMS-EMOA
13	150	10	10	20	80	SMS-EMOA
14	150	10	10	30	90	SMS-EMOA
15	150	10	10	10	30	CMA-ES
16	150	10	10	15	45	CMA-ES
17	150	10	10	20	60	CMA-ES
18	150	10	10	20	80	CMA-ES
19	150	10	10	-	30	fminsearchbnd
20	150	10	10	-	40	fminsearchbnd
21	150	10	10	-	50	fminsearchbnd

The simulated control duration for all tests is kept constant and set to 150 days. This

should be enough time to find the optimal substrate feed and to maintain the feed at the optimum so that stationarity and stability can be examined.
As initial state vector $\boldsymbol{x}(t_0)$ the steady state corresponding to the initial substrate feed (see Table 9.2) is chosen. An exception is test I.D, because there the initial feed leads to the washout state (all biomass is washed out and therefore no biogas is produced anymore). So tests I.D are started in a transient state that is very close to a point of no return.

9.3.3.2 Results

Do we find the true steady-state Pareto front? From a practical point of view this question can be answered with yes. In Figure 9.5 the steady-state Pareto front resulting out of all performed tests in experiment I together with two extensive open loop optimization runs (SMS-EGO with $n_{\text{eval}} = 750$ and $n_{\text{eval}} = 900$, respectively) is shown. To make the MONMPC test results comparable to the results of the two optimization runs the steady-state Pareto front is determined by predicting the final Pareto optimal set of each MONMPC test for 600 days. As the simulated control duration of each test is 150 d, the total prediction horizon is 750 d and therefore equal to the prediction horizon of the two optimization tests, see eq. (9.14). In Figure 9.5 it can be seen that almost all simulation results are very close to the obtained steady-state Pareto front. However, looking at the performance of the MONMPC tests with respect to different parameters some differences can be observed, which are pointed out in the following.
In Figure 9.6 results for the tests I.A and I.C and in Figure 9.7 results for the tests I.B and I.D with respect to the prediction horizon T_{p} are visualized. The tests A/C and B/D are separated in two figures, because a different behavior can be observed for both groups. The lower boundaries (for the hypervolume indicator I_{H} upper boundary) of the plots are set to the optimal values gotten from the optimal Pareto front approximation shown in Figure 9.5. In the left plot of both figures the one-dimensional stage cost $F_{1\text{D}}$ (see eq. (7.71)), obtained at the end of the 750 d long prediction, is shown. Note, that the obtained one-dimensional steady-state stage cost $F_{1\text{D}}$ is the one the control really selects based on the information 150 d $+ T_{\text{p}}$ and not the one the control would select if it knows to which steady states all feeds in the final Pareto optimal set would lead (information: 750 d). Thus, the one-dimensional steady-state stage cost $F_{1\text{D}}$ is not just the optimal one-dimensional criterion of the steady-state Pareto front. In both Figures 9.6 and 9.7 it can be seen that the one-dimensional steady-state stage cost $F_{1\text{D}}$ improves with an increasing prediction horizon T_{p}, but only until a value for T_{p} of about 200 d. This seems about right, because the ones with a shorter prediction horizon are not foresighted enough and the ones with a larger T_{p} do not focus enough on the present situation. In the left plot of Figure 9.7 the disadvantage of a control

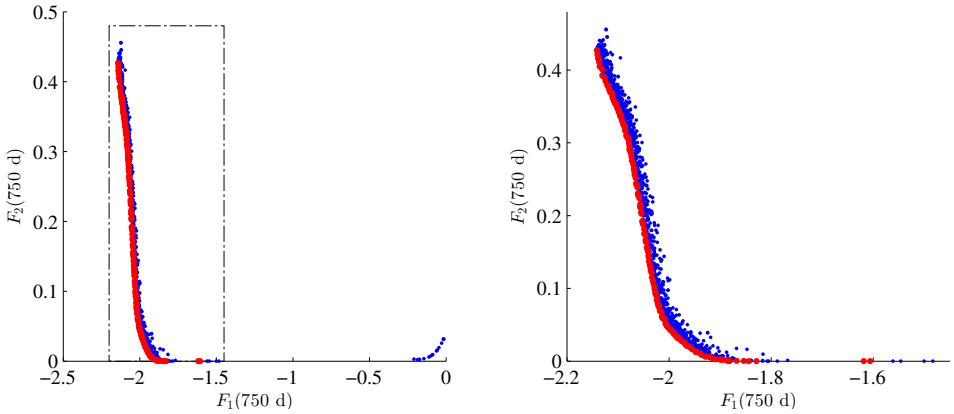

Figure 9.5: Optimal steady-state Pareto front approximation resulting out of all tests performed in experiment I. The blue dots belong to all experiments. The little bit larger red dots belong to the Pareto front of the set of all blue dots. Be aware that the steady-state Pareto front is not equal to the Pareto front of the final iteration of an MONMPC test. The first one is created out of the steady-state stage cost $\boldsymbol{F}(750\text{ d})$, where as the latter one out of the objective function $\boldsymbol{J}$ evaluated at steady state: $\boldsymbol{J}(150\text{ d} + T_\mathrm{p})$. The right plot is a zoom of the rectangular area in the left plot.

with a high prediction horizon T_p can be seen at the example of initial feed I.D. There, the biogas plant model crashes for $T_\mathrm{p} = 300$ d (test I.D5), because the control chooses a feed that is successful only in the long run. This feed works inside the optimization problem, but due to numerical inaccuracies it does not work when it is applied to the model (or the real biogas plant)[3]. A crash of a biogas plant can easily be detected by a drop of pH value and methane production, see Figure 9.12.

This behavior of a biogas plant is also the reason why a dynamic model is used inside the RTO scheme and not a static model. As a static model does not consider the current state of the plant it will suggest feeds that will only be successful in the long run but that lead to a failure of the biogas plant before. Using a static model for prediction it is very likely that almost all tests in experiment I.D would have failed. For the other three experiments I.A to I.C a static model might be sufficient.

In the middle left part of Figures 9.6 and 9.7 the hypervolume indicator I_H (Def. 3.1) of both experiment pairs A/C and B/D is shown. In Figure 9.6 the hypervolume indicator I_H is quite large, independent of the prediction horizon T_p. In Figure 9.7 it can be observed, that the hypervolume indicator I_H increases with an increasing prediction horizon T_p with the only exception of test I.D5, see the previous discussion. This was to be expected, because the initial feeds A/C are quite near the optimal substrate feed where as to find the trajectory from the initial feeds B/D to the optimal one is much

[3]The optimization algorithm is not robust, see (Beyer and Sendhoff, 2006, Kruisselbrink, 2012) for robust optimization.

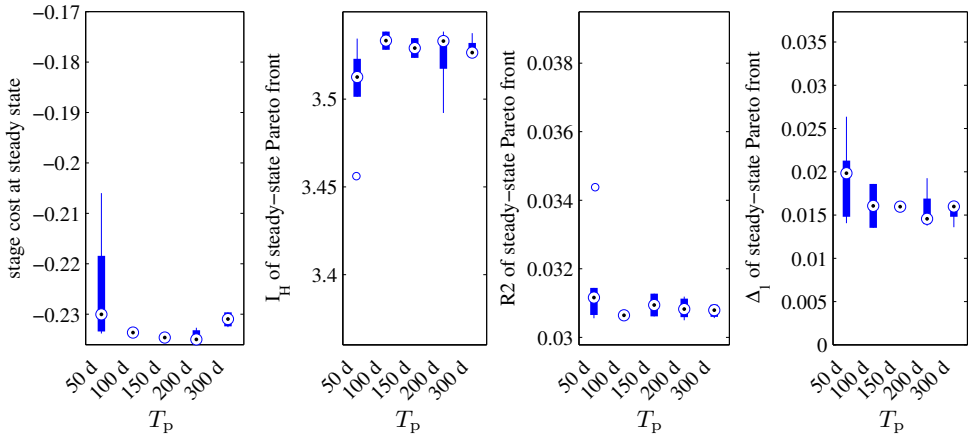

Figure 9.6: Dependency of the test results A/C on the prediction horizon T_p for the method SMS-EGO. Data from tests I.A1 until I.A5 and I.C1 until I.C5 are used. Therefore, the control horizon $T_\mathrm{c} = 10$ d and the number of simulations $n_\mathrm{eval} = 50$ are constant. Left: One-dimensional steady-state stage cost F_1D at day 750. Middle left: Hypervolume indicator I_H of the steady-state Pareto front. Middle right: R2 indicator of the steady-state Pareto front. Right: Δ_1 indicator of the steady-state Pareto front.

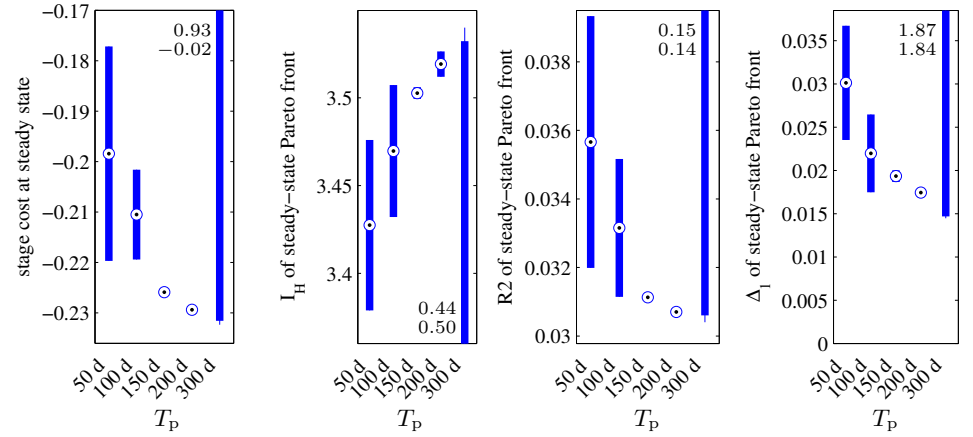

Figure 9.7: Dependency of the test results B/D on the prediction horizon T_p for the method SMS-EGO. This is the equivalent to Figure 9.6 for the tests I.B and I.D. Both tests I.D5, which is repeated once, lead to very poor results, which are outside the visualized region ($T_\mathrm{p} = 300$ d).

harder and therefore more dependent on a proper choice of the prediction horizon T_p. The same is about true for the trends of the R2 and Δ_1 indicator, shown in both Figures 9.6 and 9.7 middle right and right, respectively.

The comparison of the results for the optimization methods in Figure 9.8, based on the one-dimensional steady-state stage cost F_1D (left), shows that SMS-EGO performs significantly better than SMS-EMOA. This is in contrast to the values of F_1D in

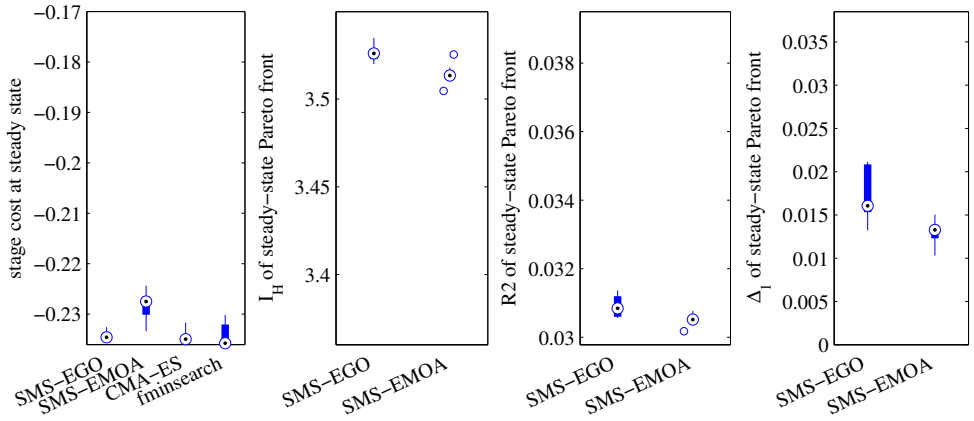

Figure 9.8: Dependency of the test results A/C on the optimization method. Data from tests I.A3, I.A7, I.A8 and I.A11 until I.A21 as well as I.C3, I.C7, I.C8 and I.C11 until I.C21 are used. In these plots prediction horizon $T_\mathrm{p} = 150$ d and control horizon $T_\mathrm{c} = 10$ d. Left: One-dimensional steady-state stage cost F_1D at day 750. Middle left: Hypervolume indicator I_H of the steady-state Pareto front. Middle right: R2 indicator of the steady-state Pareto front. Right: Δ_1 indicator of the steady-state Pareto front.

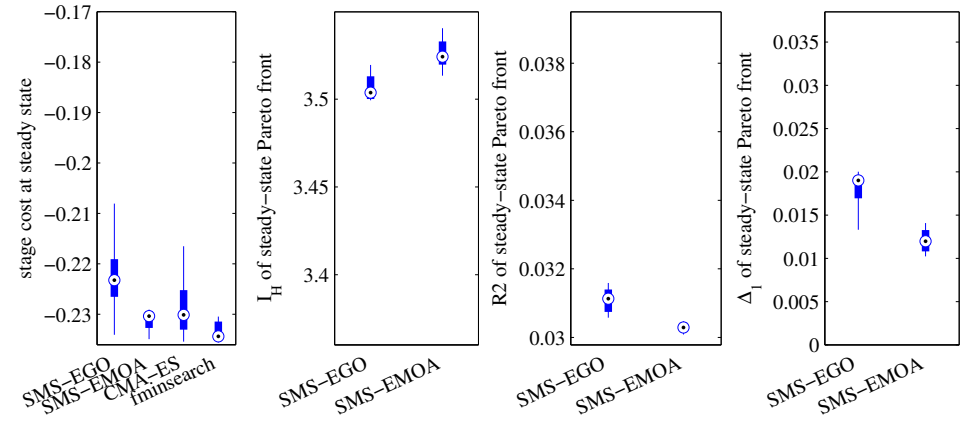

Figure 9.9: Dependency of the test results B/D on the optimization method. This is the equivalent to Figure 9.8 for the tests I.B and I.D. Test I.B20 (fminsearch) failed and therefore is not visualized in the plot.

Figure 9.9, where SMS-EMOA is clearly superior to SMS-EGO. With respect to the hypervolume indicator I_H, R2 and Δ_1 indicator, SMS-EMOA yields better results than SMS-EGO in five of six cases for all four categories A until D.

The number of simulations n_eval performed in SMS-EMOA and CMA-ES are chosen so that the total runtime of one test approximately lasts the same amount of time as a test using SMS-EGO does. About 77 % of all tests used to compare the optimization methods in experiment I (49 of 64 tests) are performed on computer 1 (see Section

9.3). There, the median of the runtime of a test using SMS-EGO as method lasts 16.9 h and for SMS-EMOA the median runtime is 15.6 h. With a median of 20.6 h the tests using CMA-ES last a little bit longer, but CMA-ES yields better one-dimensional steady-state stage cost F_{1D} results at least for tests A/C, see Figure 9.8. Surprisingly, the simplex method (fminsearch) with a median runtime of 16.9 h offers the best results. It seems to be that the objective function in this configuration does not have many local optima so that the locally converging simplex method provides such good results. Nevertheless, it cannot be guaranteed that the simplex method finds the global optimum if the configuration of the objective function is changed. This is why the simplex method is used out of competition and therefore is not further investigated in the following experiments. However, the simplex method can be used as a dual method or "polisher" to improve optimization results found by a global optimization method such as CMA-ES.

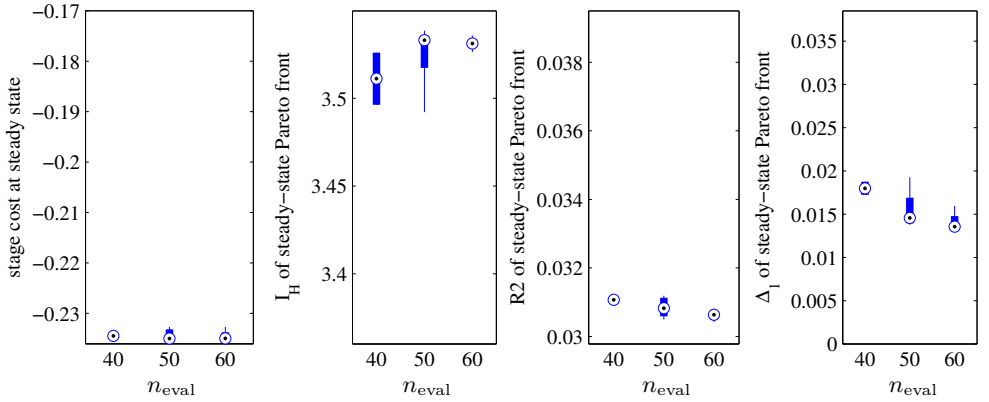

Figure 9.10: Dependency of the test results A/C on the number of simulations n_{eval}. Data from tests I.A4, I.A9 and I.A10 as well as I.C4, I.C9 and I.C10 are used, thus $T_p = 200$ d. Left: One-dimensional steady-state stage cost F_{1D} at day 750. Middle left: Hypervolume indicator I_H of the steady-state Pareto front. Middle right: R2 indicator of the steady-state Pareto front. Right: Δ_1 indicator of the steady-state Pareto front.

For the number of simulations n_{eval} in each iteration no clear trend can be seen in both Figures 9.10 and 9.11 for the one-dimensional steady-state stage cost F_{1D}. It seems that for a good steady-state solution enough simulations (150 d/$\delta \cdot n_{eval}$) are performed for all selected number of simulations n_{eval}. The quality of the obtained Pareto front, measured by the three performance measures I_H, R2 and Δ_1, appears to increase with the number of objective function evaluations, at least in five of six cases (the trend of the hypervolume indicator in Figure 9.10 is not counted).

The control horizon (test I.4 vs. test I.6, $T_c = 10$ d vs. $T_c = 5$ d) has not such a large influence on the steady-state solution. The fact that in test I.6 due to the control

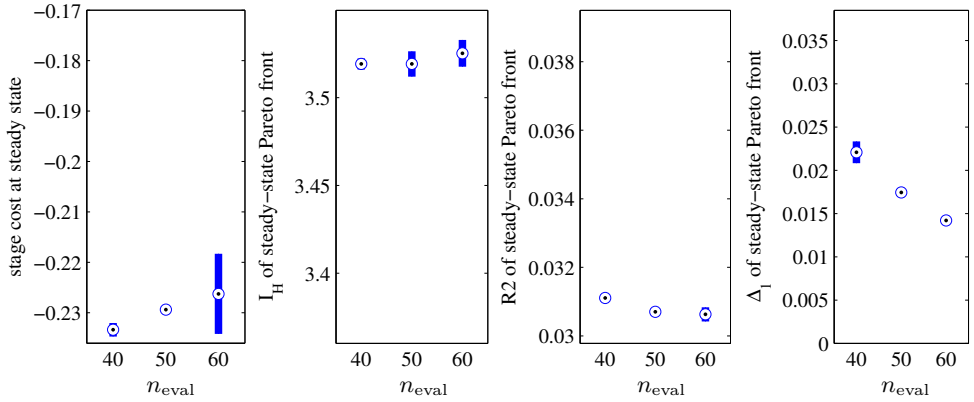

Figure 9.11: Dependency of the test results B/D on the number of simulations n_{eval}. This is the equivalent to Figure 9.10 for the tests I.B and I.D.

horizon twice as many simulations are performed as in test I.4 makes the results of test I.6 most of the time a little bit better than the ones of test I.4. Nevertheless, it can be expected that the influence of the control horizon in the setpoint experiment III is more apparent, see Section 9.3.5.

Size of the basin of attraction of the true steady-state Pareto front? Based on the optimal Pareto front approximation seen in Figure 9.5 it can be concluded that all selected initial feeds I.A to I.D (see Table 9.2) belong to the basin of attraction of the true steady-state Pareto front. This result is quite remarkable because the chosen initial feeds are taken from a quite large range of values. Dependent on the control parameters it can happen that a Pareto front approximation is obtained that is not as good as the true one. But in general it is possible to find the true steady-state Pareto front from each initial state.
If it is possible to reach the steady-state Pareto front from almost every initial state it means that the steady-state solution does not depend on the feed trajectory leading to the steady-state. In other words the steady-state solution only depends on the final substrate feed and not on the previous feed values. This means that using NMPC we will not find more optima as we can find using open loop optimization. At least the obtained results indicate that this observation could be true.

Stability of the closed loop? To test whether the control is stationary in Figure 9.13 the absolute change of the total substrate feed over the simulated control duration is shown. It can be seen that all controls are stationary. Only a very few controls change the feed after the 100th simulated day.
Note that in all tests above a perfectly known plant was assumed with no plant-model mismatch, measurement noise or drift. Here, the first five tests for experiments I.B and

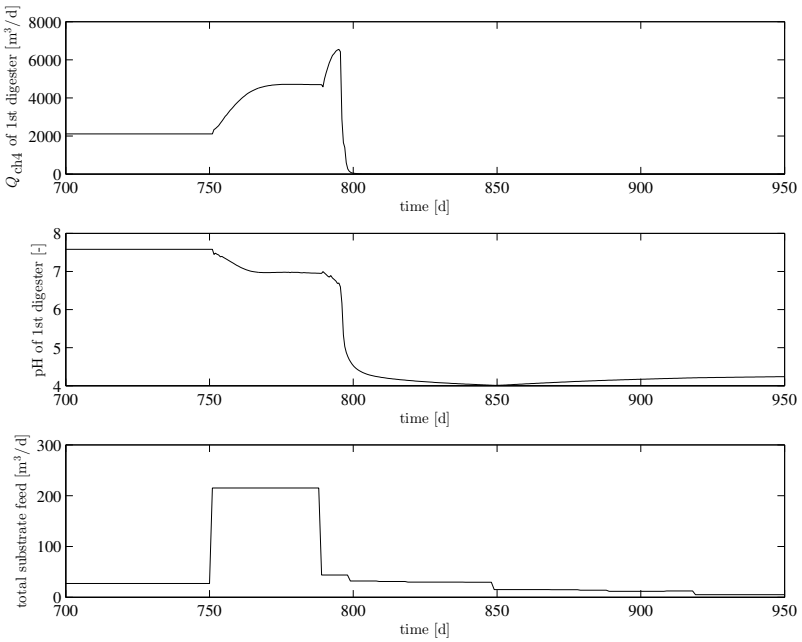

Figure 9.12: Simulation results for test I.D5. At hand of the methane production Q_{ch_4} and the pH value of the 1st digester one can see, that the digester fails. The total substrate feed in the lowest plot is the sum of the volumetric flow rate of the three fed substrates maize silage, swine manure and grass silage.

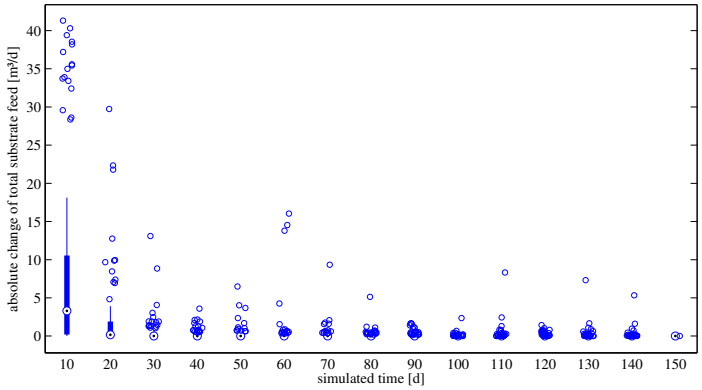

Figure 9.13: Absolute change of total substrate feed over the simulated control duration. The data of all tests in experiment I for the ideal model is used. It can be seen that all controls are stationary.

I.D (Table 9.3) are repeated with a not perfectly known controlled model (see Section 9.3.2). The results are depicted in Figure 9.14 in the same format as they are visualized in Figure 9.7 for the ideal world results.

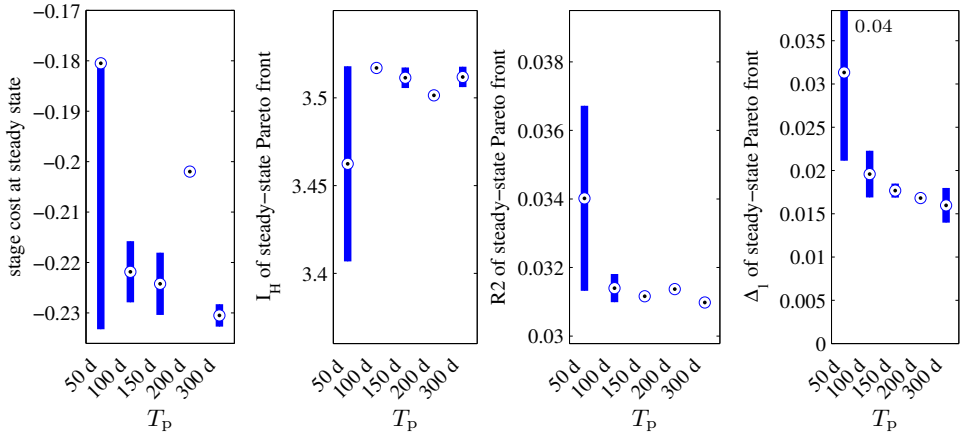

Figure 9.14: Dependency of the test results B/D on the prediction horizon T_p for the method SMS-EGO. This is the equivalent to Figure 9.7, but this time in a noisy environment created in Section 9.3.2. Solving the ADM1 in a non-stationary environment is numerically difficult. Because of that test I.B4 failed three times and therefore is not displayed. Left: One-dimensional steady-state stage cost F_1D at day 750. Middle left: Hypervolume indicator I_H of the steady-state Pareto front. Middle right: R2 indicator of the steady-state Pareto front. Right: Δ_1 indicator of the steady-state Pareto front. The Δ_1 indicator for test I.D1 is short outside the visualized region ($T_\mathrm{p} = 50$ d).

The initial feeds I.B and I.D are very far away from the optimal feed (see Table 9.2). Therefore, it is not unexpected that the steady-state results in a noisy environment for both initial feeds are different to the results in the ideal world. By comparing Figures 9.7 and 9.14 it can be seen that the results are not that different. With respect to the one-dimensional steady-state stage cost F_1D only test I.D4 ($T_\mathrm{p} = 200$ d) yields a considerable different result. The trend of the hypervolume indicator of the steady-state Pareto front looks different. Here indeed test I.D2 ($T_\mathrm{p} = 100$ d) and again test I.D4 ($T_\mathrm{p} = 200$ d) have different results. The trends of the R2 and Δ_1 indicator are very much alike, this is especially true for the Δ_1 indicator. In conclusion one can say that the RTO is quite robust against noise and plant-model mismatch. Be aware that the plant-model mismatch is still there at steady state whereas the noise is not.

Can the results be repeated? For experiment I in total 16 tests are repeated once and three tests are repeated twice. The median of the absolute values of the variation of the steady-state stage cost $F_\mathrm{1D}(750\text{ d})$ in those repetitions is 0.0004. In comparison, the absolute median variation of the steady-state stage cost $F_\mathrm{1D}(750\text{ d})$ in all tests of experiment I is 0.0024. For the hypervolume indicator (R2, Δ_1 indicator) these numbers are for the repetitions 0.0030 (0.0001, 0.0009) and 0.0095 (0.0003, 0.0027) for all tests. Based on these numbers, the variation in the repetitions can be seen as reasonably small compared to the total variation of the four measures. Therefore, the obtained

results seem to be repeatable.

Optimal feeds and parameter sets In Figure 9.15 the optimal, with respect to the fitness J_{1D}, substrate feeds taken out of the final approximation of the Pareto optimal set are shown. All feeds qualify for the manure bonus (see Section 7.3.2), it also can be seen that all substrate mixtures contain a little more manure than would be required for the bonus. In the upper left view it can be observed that all feeds almost lie on one line. When maize silage is decreased, grass silage is increased.

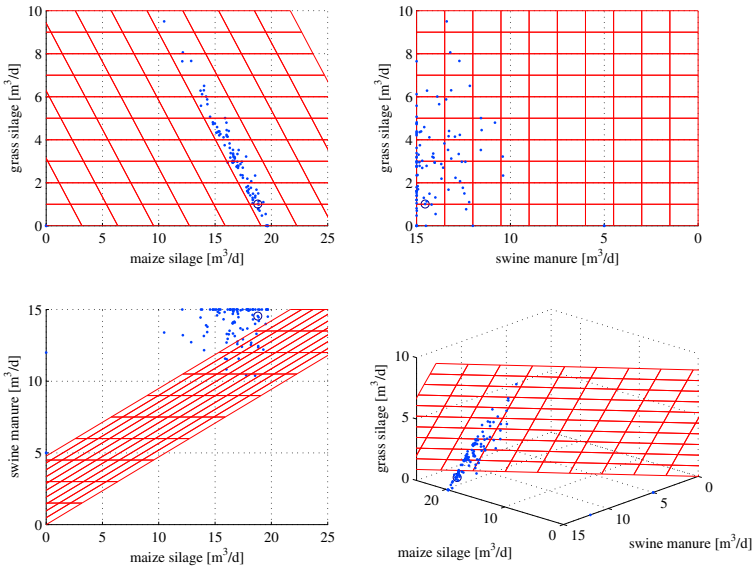

Figure 9.15: With respect to fitness J_{1D} optimal substrate feeds of the final approximation of the Pareto optimal set obtained in experiment I. The feeds are visualized in three views. Top left: Front view, top right: Left view, bottom left: Top view and bottom right: 3D view. The red plane divides the feeds in those which qualify for the manure bonus (see Section 7.3.2) and those who do not. The optimal feed, with respect to the one-dimensional steady-state stage cost F_{1D}, is emphasized by a circle.

With respect to the one-dimensional steady-state stage cost F_{1D} the best performing test in experiment I is test I.A21 (fminsearch) with a value of $F_{1D}\,(750\text{ d}) \approx -0.2361$. The corresponding optimal substrate mixture contains out of 18.79 $\frac{\text{m}^3}{\text{d}}$ maize silage, 14.54 $\frac{\text{m}^3}{\text{d}}$ swine manure and 1.01 $\frac{\text{m}^3}{\text{d}}$ grass silage, which is also visualized in Figure 9.15 by a circle. The absolute best value ever obtained for the one-dimensional steady-state stage cost is $F_{1D}\,(750\text{ d}) \approx -0.2363$. It was found in an optimization run. The corresponding feed is 18.73 $\frac{\text{m}^3}{\text{d}}$ maize silage, 14.99 $\frac{\text{m}^3}{\text{d}}$ swine manure and 0.97 $\frac{\text{m}^3}{\text{d}}$ grass silage. Thus, both feeds are almost exactly the same.

Among the three global optimization methods the best test is I.A16 (CMA-ES) with a

value of F_{1D} (750 d) ≈ -0.2359. The corresponding optimal substrate mixture contains out of 19.68 $\frac{m^3}{d}$ maize silage, 15.00 $\frac{m^3}{d}$ swine manure and 0.00 $\frac{m^3}{d}$ grass silage.
The best value for the hypervolume indicator I_H is obtained in test I.B12 with a value of $I_H \approx 3.5405$. The best test for the other two indicators R2 and Δ_1 is I.D12. Their values are R2 ≈ 0.0301 and $\Delta_1 \approx 0.0102$. In both tests SMS-EMOA is used as optimization method. It is interesting to see that the best steady-state Pareto front approximations are found when starting at the most difficult initial substrate feeds I.B and especially I.D.
The strength of the multi-objective optimization methods are that they return a set of optimal solutions from which the decision maker can pick a solution. But, if the applied solution is always chosen by predefined weights a single-objective method such as CMA-ES may yield better results. The problem of the used multi-objective methods is that they rather try to approximate the complete Pareto front, thus also its extremes, and do not concentrate their search in the region where the single-objective weighted criterion is optimized. Thus, the strength of the multi-objective solutions is only exploited well when based on the given Pareto front it is decided which solution is picked and not beforehand.

9.3.4 Experiment II: Change of Substrate Mixture

A sudden change in the substrate mixture of a biogas plant can often result in a transient decrease in performance (e.g. leaving a setpoint) or even lead to process instabilities or failure. Using predictive control such an adjustment of the fed substrates can be made smoothly and thus above mentioned disadvantages can be avoided. Such a scenario is investigated in this second experiment, where the substrate feed has to be changed because the substrate maize silage will be used up during the simulated control duration. Despite the change of the substrate mixture the control has to carry on tracking a given methane setpoint $Q^*_{ch_4,ext}(t)$. Furthermore, the new substrate mixture should also be optimal for the biogas plant given the limited amount of substrates available.

9.3.4.1 Setup

In a first test it will be evaluated what happens if the depletion of maize silage is not taken into account during prediction. This should be the worst case scenario. Then tests are done where the decreasing amount of maize silage in the silo is used as a further information during prediction. This is implemented by changing the upper boundary UB_{i_u} for the i_uth substrate so that the amount given by the upper boundary could be fed for the complete duration of some future horizon. The length of this future horizon is difficult to determine. If it is set to the prediction horizon the fed amount of the limited substrate will be very low if the prediction horizon is long. An optimal solution

for the horizon could not be determined in this thesis so it is set by experience to $\frac{T_\mathrm{p}}{4}$, but at least to a value of 14 d. To avoid that shortly before the substrate is depleted only very small amounts of the substrate are fed the corresponding upper boundary $\mathrm{UB}_{i_\mathrm{u}}$ is limited to a minimal value of 2 $\frac{\mathrm{m}^3}{\mathrm{d}}$.
The prediction horizon T_p is the only control parameter which is evaluated in this experiment, using values 50 d, 100 d and 150 d. All tests are started with the optimal substrate feed found in test I.A16, which is $Q_\mathrm{maize} \approx 19.68\ \frac{\mathrm{m}^3}{\mathrm{d}}, Q_\mathrm{manure} = 15.00\ \frac{\mathrm{m}^3}{\mathrm{d}}$ and $Q_\mathrm{grass} = 0.00\ \frac{\mathrm{m}^3}{\mathrm{d}}$. The assumed amount of maize silage in the silo at the start of the simulation is 1000 t. The other two substrates swine manure and grass silage are not finite in time.
The simulated control duration is set to 300 days and the control is started at day 20. At day 160 the maize silage silo is refilled, so that the control has the task to return to the optimal substrate feed where it started from.
In this experiment the two best controller configurations obtained in experiment I are used, except of the different value for the prediction horizon T_p. They are the configuration I.12 using SMS-EMOA and I.16 using the method CMA-ES, see Table 9.3.
In order that during the simulated control duration the methane setpoint $Q^*_{\mathrm{ch}_4,\mathrm{ext}}(t)$ is hold, the objective function $\boldsymbol{J}$ is extended by a setpoint term. This term is used in experiment III as well and is described there, see Section 9.3.5. In this experiment a constant CH_4 setpoint is used with a value of $Q^*_{\mathrm{ch}_4,\mathrm{ext}}(t) = 2797.5\ \frac{\mathrm{m}^3}{\mathrm{d}}$. This amount of methane is produced with the initial feed all tests are started from.

9.3.4.2 Results

In Figure 9.16 the obtained results for configuration I.16 and $T_\mathrm{p} = 150$ d with and without including the available amount of maize silage in the silo are compared.
In Figure 9.16 it can be seen that the "hard" control, which changes the feed in a moment, tracks the methane setpoint very poorly during the transition. The reasons are the fast change of the feed but also the delayed switch to the usage of grass silage. The reason is, that once the setpoint error is larger than an upper boundary the fitness value is cut-off by the Tukey's biweight function (see eq. (9.16)). Therefore, a reasonable control error and a huge one are rated the same. The reason is that the control should be able to leave a setpoint if it is beneficial for the biogas plant. As a high amount of grass silage leads to an increase of ammonia the control prefers to loose the setpoint for a while and only later (at day 110) changes the feeding regime to a higher amount of grass silage.
At the time maize silage is available again (day 160), the "smooth" control immediately changes back to a by maize silage dominated feed. This comes with a little overshoot of methane production. Furthermore, it can be observed that both controls do not

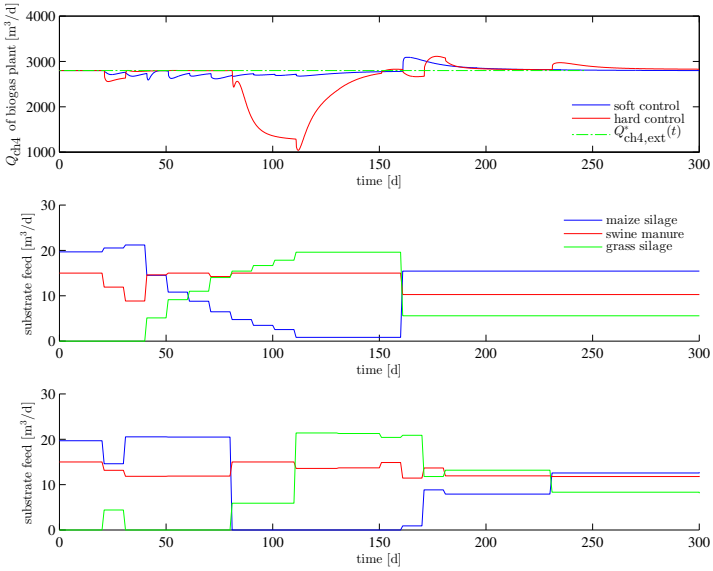

Figure 9.16: Comparison of controls with and without inclusion of the available amount of maize silage in the silo during prediction for configuration I.16 and $T_\mathrm{p} = 150$ d. Top: Methane production of the biogas plant and methane setpoint $Q^*_{\mathrm{ch}_4,\mathrm{ext}}(t)$. Middle: Substrate feed of the control with prediction of the available feed stock ("soft" control). Bottom: Substrate feed of the control without prediction of the available feed stock ("hard" control).

return to the substrate mix they started from, resulting in a worse one-dimensional steady-state stage cost F_1D compared to the one at initial state as can be seen in Figure 9.18 below.

In Figure 9.17 the same presentation as in Figure 9.16 is shown. Again configuration I.16 is used, but this time with a prediction horizon of $T_\mathrm{p} = 50$ d. Here, the hard control is not that much worse than the soft control by just looking at the control error $e_{\mathrm{ch}_4,\mathrm{ext}}(t)$ (see eq. (9.15)). The reason is that the first one is better and the latter one is worse than the ones for $T_\mathrm{p} = 150$ d shown in Figure 9.16. For both controls the final substrate feed is almost the same as the initial one. Therefore, for this configuration the control almost returns to the optimal feed it started from.

In the top row of Figure 9.18 the obtained fitness values at the end of the simulated control duration J_1D (300 d) is shown. It can be seen that the fitness value for the soft control is most of the time worse than the one of the hard control. This was not expected but can be explained as follows. With the change to a grass silage dominated feed the ammonia, VFA and VFA/TA contents in the digesters increase. All three influence the fitness value negatively (the fitness value increases). As changing the feed leads to loosing the methane setpoint for a short while it is not beneficial for the soft control to leave the setpoint improving the fitness on a longer term. Only when the

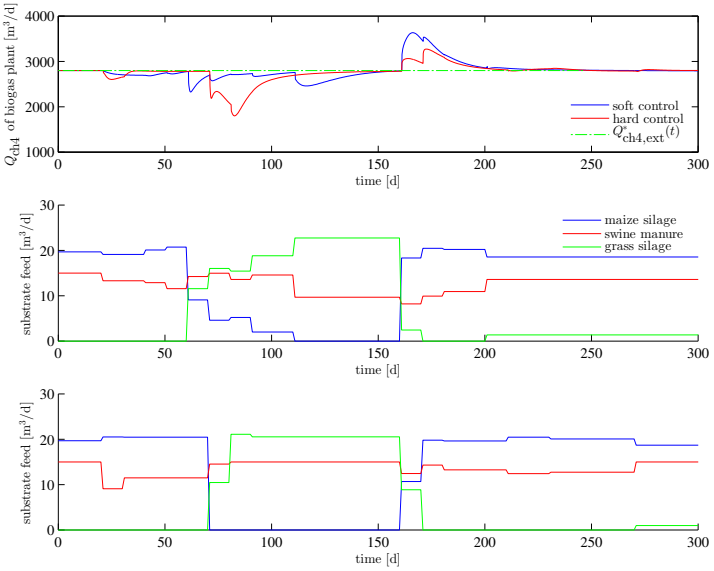

Figure 9.17: Comparison of controls with and without inclusion of the available amount of maize silage in the silo during prediction for configuration I.16 and $T_\mathrm{p} = 50$ d. Top: Methane production of the biogas plant and methane setpoint $Q^*_{\mathrm{ch}_4,\mathrm{ext}}(t)$. Middle: Substrate feed of the control with prediction of the available feed stock ("soft" control). Bottom: Substrate feed of the control without prediction of the available feed stock ("hard" control).

setpoint is already lost (hard control) the control has the freedom to leave the setpoint even more, because the fitness value corresponding to the control error is cut-off (see above).

In the middle row of Figure 9.18 the one-dimensional steady-state stage cost F_1D (500 d) is shown. Here again, the soft control is worse than the hard control. This is due to the fact that the final substrate feed of the hard control is most often better than the one of the soft control.

For SMS-EMOA the reason for this is that the soft control does not change the feed at day 160 at all. Therefore, maize silage is kept at 0 $\frac{\mathrm{m}^3}{\mathrm{d}}$. In Figure 9.19 the reason for that behavior can be observed. There, the populations shortly before and at the time maize silage is available again (day 160) are plotted for configuration I.12 with $T_\mathrm{p} = 150$ d. It can be observed that the solution candidates of the soft control are only located at the currently optimal feed and nowhere else. The versatility in feeds for the hard control is much higher. This is because the soft control sets the amount for maize silage at an earlier stage to 0 $\frac{\mathrm{m}^3}{\mathrm{d}}$ as does the hard control. Therefore, the versatility in solutions is lost over the last number of iterations. This urged population is the reason why at day 160 SMS-EMOA cannot generate new and different solutions because the population does not allow space for exploration. Here, it can be seen that initializing

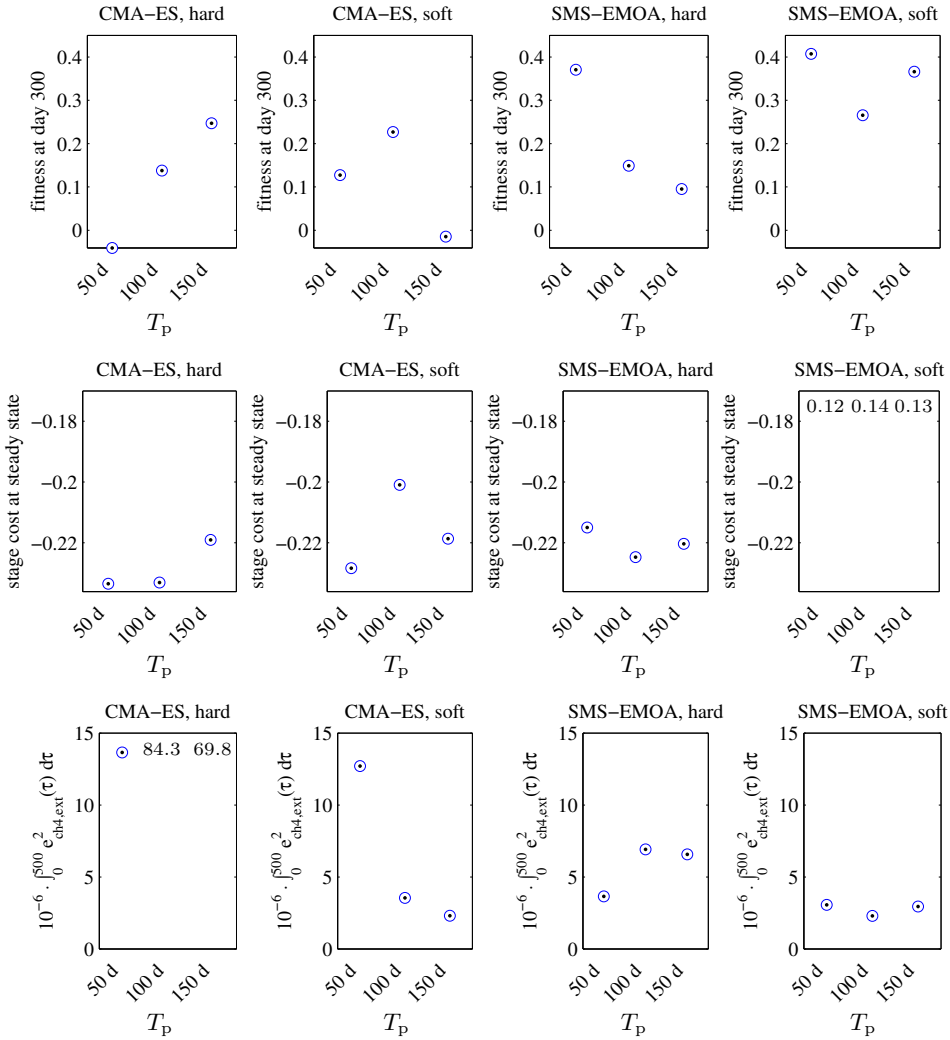

Figure 9.18: Obtained results for fitness at the end of the simulated control duration (J_{1D} (300 d), top row), one-dimensional steady-state stage cost (F_{1D} (500 d), middle row) and the integral of the squared control error over 500 days: $10^{-6} \cdot \int_0^{500} e^2_{ch_4,ext}(\tau)\,d\tau$, bottom row. The figure compares the two optimization methods CMA-ES (config. I.16) and SMS-EMOA (config. I.12) as well as the inclusion of the feed stock during prediction (soft) and not (hard). The steady-state stage cost results for SMS-EMOA (soft) are out of the visualized region. This is also true for the tracking error obtained with CMA-ES (hard) for $T_p = 100$ d and $T_p = 150$ d.

SMS-EMOA only with the last population without any randomly generated solution candidates is a bad strategy (see Section 9.3.1). By replacing some solution candidates in the initial population by randomly (or LHS) selected candidates it can be expected that much better results are obtained. This is not done here to avoid that all tests

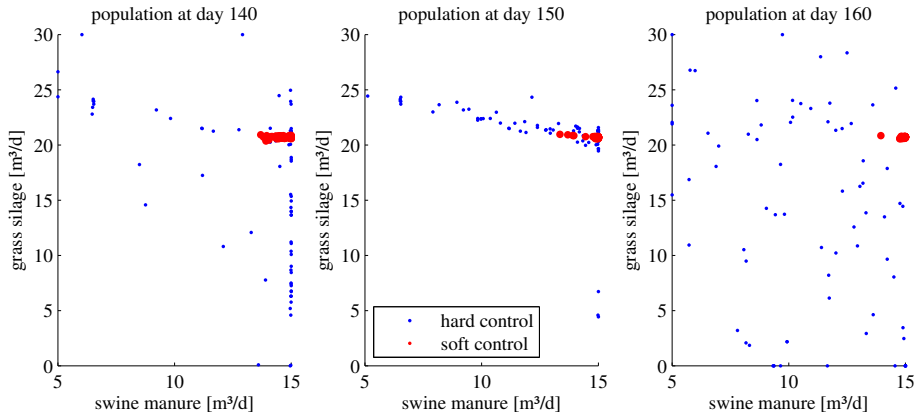

Figure 9.19: Comparison of the final populations of individuals from day 140 to day 160 (from left to right) for configuration I.12 (SMS-EMOA) with $T_\mathrm{p} = 150$ d. The red dots for the soft control are plotted a little bit larger so that they can be located easier. It can be seen that the versatility of the solution candidates of the hard control is much higher compared with the soft control.

performed so far have to be repeated.

For CMA-ES the reason that the one-dimensional steady-state stage cost for the soft control is worse compared to the one for the hard control might be that at day 160 the soft control tracks the setpoint a little bit more accurate and therefore has more difficulty to leave it for a longer time.

In the bottom row of Figure 9.18 the integral of the squared control error over 500 days, $10^{-6} \cdot \int_0^{500} e^2_{\mathrm{ch_4,ext}}(\tau)\,\mathrm{d}\tau$, is shown. It can be seen that the soft control always yields better setpoint tracking results. For CMA-ES the hard control is very bad for $T_\mathrm{p} = 100$ d and $T_\mathrm{p} = 150$ d as could also be seen in Figure 9.16 above.

In this experiment no tests in the noisy environment are performed. The reason is that all tests in this experiment are computationally very expensive and performing them in the noisy environment would blast the performance of the available PCs.

The winning configuration of this experiment is the soft implementation of I.16 with $T_\mathrm{p} = 150$ d. Thus, it is exactly configuration I.16 from Table 9.3 that was already the winner in experiment I.

Especially the soft control using configuration I.12 (SMS-EMOA) is a complete disappointment. At least the hard controls using SMS-EMOA for $T_\mathrm{p} = 100$ d and $T_\mathrm{p} = 150$ d yield somehow satisfying results.

9.3.5 Experiment III: Setpoint Control

In this third experiment the real-time optimization scheme is used as setpoint tracking control. In the tests performed here, the control variable is the volumetric flow rate of methane $Q_{\mathrm{ch_4}}(t)$ which has to follow a given methane setpoint $Q^*_{\mathrm{ch_4,ext}}(t)$. Therefore,

the objective function $\boldsymbol{J}$ in Section 7.3.4 is extended by a term measuring the control error $e_{\mathrm{ch}_4,\mathrm{ext}}(t)$, defined in eq. (9.15).

$$e_{\mathrm{ch}_4,\mathrm{ext}}(t) := Q^*_{\mathrm{ch}_4,\mathrm{ext}}(t) - Q_{\mathrm{ch}_4}(t) \tag{9.15}$$

More precisely the second component of the stage cost function F_2 given in eq. (7.66) is extended by the control error $e_{\mathrm{ch}_4,\mathrm{ext}}(t)$ by introducing a further constraint. This additional constraint is modeled as

$$\mathrm{constraint}_{n_c+1}(\tau) := \rho_{\mathrm{Ty}}\left(\zeta \cdot e^2_{\mathrm{ch}_4,\mathrm{ext}}(\tau)\right) \tag{9.16}$$

with Tukey's biweight function ρ_{Ty} (7.69) and a weight $\zeta \in \mathbb{R}^+$. The weight ζ is used to scale the squared control error $e^2_{\mathrm{ch}_4,\mathrm{ext}}(\tau)$ to the sensitive domain of Tukey's biweight function ρ_{Ty}.
Note the difference between the control error $e_{\mathrm{ch}_4}(t)$ and the "external" control error $e_{\mathrm{ch}_4,\mathrm{ext}}(t)$. The first one is minimized by the process control and the latter one by the NMPC.

9.3.5.1 Setup

The setpoint trajectory $Q^*_{\mathrm{ch}_4,\mathrm{ext}}(t)$ used in the tests is characterized by two 100 d long constant periods and only two steps over the complete scenario (see Figure 9.20). The special property of the trajectory is that the setpoint at the start and the end of the scenario are the same and the setpoint in between is very bad for the biogas plant. Based on this trajectory the ability of the control to find and maintain a steady-state solution for a given setpoint and to find it again at a later point will be studied. To prove that the control is intelligent, it is investigated with the bad setpoint how the control behaves, because it may not just follow the setpoint. Furthermore, dynamics, oscillation, overshooting and action on the manipulated variable can be investigated in this experiment.
In the tests only the dependency of the results on the prediction horizon T_p is studied. As prediction horizon the four values $T_\mathrm{p} = 10$ d, $T_\mathrm{p} = 25$ d, $T_\mathrm{p} = 75$ d and $T_\mathrm{p} = 100$ d are chosen. The simulated control duration is set to 250 days. For all other parameters (optimization method and number of simulations) the two best configurations obtained in experiment I are used (Section 9.3.3). They are configuration I.12 with SMS-EMOA and I.16 with CMA-ES as optimization methods, see Table 9.3.
An important aspect for setpoint tracking is the performance of the control in a noisy and erroneous environment. Therefore, all tests are first performed in a perfect environment and then repeated in an environment where measurements are noisy, drifting and error-prone, a plant-model mismatch exists and substrate parameters are not exactly known (see Section 9.3.2). As the simulation studies with the real world model are computational very expensive the simulated control duration is reduced to

150 days. As setpoint a constant value of $Q^*_{\mathrm{ch4,ext}}(t) = 2750\ \frac{\mathrm{m}^3}{\mathrm{d}}$ is used, which is the same value as the previous setpoint trajectory has at the start and in the end. Next to the prediction horizon, here also the control horizon for the best configurations is changed once to $T_\mathrm{c} = 5$ d for comparison.

9.3.5.2 Results

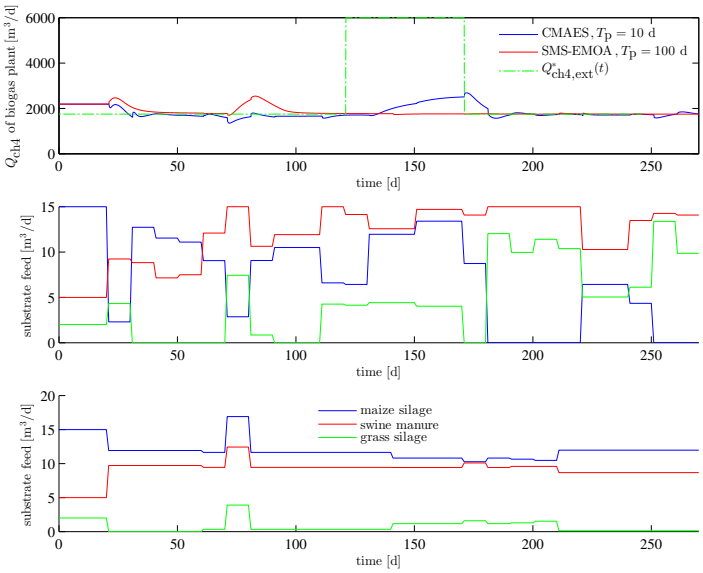

Figure 9.20: Setpoint control for ideal model: Comparison of two tests using configuration I.16 with $T_\mathrm{p} = 10$ d and configuration I.12 with $T_\mathrm{p} = 100$ d. Top: Methane production of the biogas plant with setpoint $Q^*_{\mathrm{ch4,ext}}(t)$. Middle: Substrate feed of the control with CMA-ES and $T_\mathrm{p} = 10$ d. Bottom: Substrate feed of the control with SMS-EMOA and $T_\mathrm{p} = 100$ d.

In Figure 9.20 simulation results for the setpoint tracking tests for the ideal simulation model are shown. Two controls, each with a different value for the prediction horizon, are compared. They are the best and worst performing controls in these tests. The controls are started at day 20 with an initial feed of 15 $\frac{\mathrm{m}^3}{\mathrm{d}}$ maize silage, 5 $\frac{\mathrm{m}^3}{\mathrm{d}}$ swine manure and 2 $\frac{\mathrm{m}^3}{\mathrm{d}}$ grass silage. It can be seen that both controls converge to the setpoint, which the control with the larger prediction horizon tracks more accurately and much more stable. Because of the large bump in the setpoint between day 120 and day 170 both controls only slightly leave the previous setpoint for some time. This behavior is desired, because the setpoint of 6000 $\frac{\mathrm{m}^3}{\mathrm{d}}$ is not beneficial for the biogas plant. In contrast to the control with $T_\mathrm{p} = 100$ d the one with the short prediction horizon fails to find a stationary substrate feed. Furthermore, the final feed for $T_\mathrm{p} = 10$ d is totally different to the nearly optimal one obtained for $T_\mathrm{p} = 100$ d. The latter substrate feed is

almost as good as the best one found in the tests below which can be seen as reference values (see Figure 9.23). With respect to the one-dimensional steady-state stage cost the difference between both optimal solutions is only 0.0034. Therefore, one can say that the control is able to find the optimal substrate feed while tracking a setpoint. But this wanted behavior is highly dependent on the prediction horizon as can be seen in Figure 9.21.

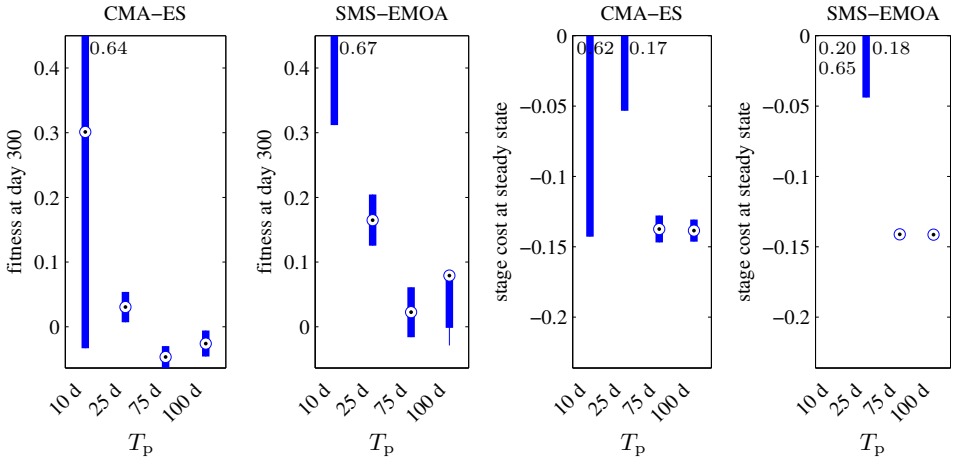

Figure 9.21: Setpoint control for ideal model: Results for fitness at the end of the simulated control duration (J_{1D} (300 d), left) and one-dimensional steady-state stage cost (F_{1D} (500 d), right). Comparison of configurations I.12 and I.16 for different values of the prediction horizon T_p. The tests with $T_p = 10$ d and $T_p = 25$ d yield very bad results and therefore are partly not visualized. All tests are repeated once, one test (SMS-EMOA, $T_p = 100$ d) is repeated twice.

In Figure 9.21 all results yield in experiment III for the setpoint shown in Figure 9.20 above and with the ideal model are shown. The fitness at the end of the simulated control duration (J_{1D} (300 d)) and the one-dimensional steady-state stage cost (F_{1D} (500 d)) are visualized and compared with respect to the chosen prediction horizon T_p and optimization method. Both, fitness and steady-state stage cost in general improve with an increasing prediction horizon. There is no best configuration. However, the CMA-ES based configurations most of the time yield better fitness values and the one for $T_p = 75$ d is pretty good.

To evaluate the control's performance in a noisy environment the next test results are obtained applying the control at the real world model. As explained in the setup above a constant setpoint is used here, as can be seen in the top plot of Fig. 9.22. For comparison the same tests are also evaluated at the ideal model.

In Figure 9.22 two tests using the same configuration (I.12 with $T_p = 100$ d) are compared. In the first test the control is applied to the ideal model and in the latter

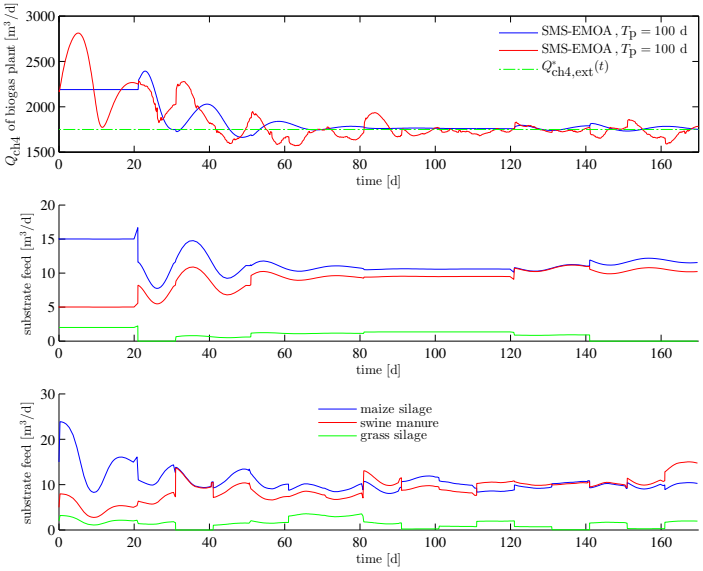

Figure 9.22: Setpoint control for real world model: Comparison of two tests using configuration I.12 with $T_p = 100$ d, one is evaluated at the ideal and the other at the real world model. Top: Methane production of the biogas plant with setpoint $Q^*_{ch_4,ext}(t)$. In blue the CH_4 production of the ideal and in red the one of the real world model is visualized. Middle: Substrate feed of the control applied to the ideal model. Bottom: Substrate feed of the control applied to the real world model.

test the control is applied to the real world model. Using the ideal model the control tracks the setpoint very well finding a stationary feed at the end (see the top and middle plot in Figure 9.22). Applied to the real world model the control is able to track the setpoint without an offset. This is due to the used process control. The NMPC itself is not able to control the plant offset-free. However, it seems that the process control is not fast enough to compensate all disturbances immediately. It is apparent that the process control in the beginning between day 0 and day 20 produces a high over- and undershoot to get to the initial setpoint. This is very unfortunate and one of the weaknesses of the used process control. The extension of the process control proposed in Section 9.2 does not have this disadvantage. It reduces the overshoot by 77 %, results are not visualized here. Note, that an overshoot of the process control is not punished harder as an undershoot. However, as in reality an overshoot could mean that the additionally produced biogas must be burned in a torch an overshoot in this case would be inferior to an undershoot. Using a model-based process control instead of Antonelli et al. (2003) better results might be expected. Nevertheless, Antonelli et al. (2003) has the advantage of its simplicity and therefore it is used here.

The final substrate mixture found for the real world model is almost the same as is

found for the ideal model. This can also be seen at the one-dimensional steady-state stage cost which is visualized in Figure 9.23 among others.

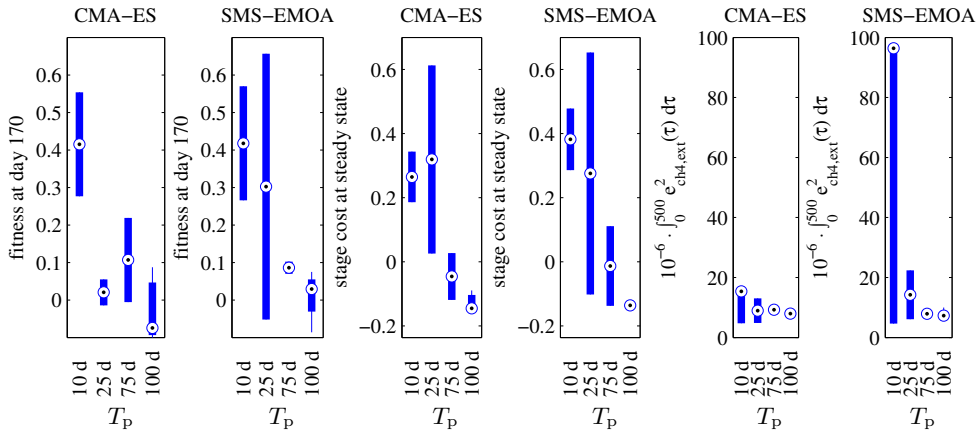

Figure 9.23: Setpoint control for ideal and real world model: Results for fitness at the end of the simulated control duration (J_{1D} (170 d), left), one-dimensional steady-state stage cost (F_{1D} (500 d), middle) and the integral of the squared control error over 500 days: $10^{-6} \cdot \int_0^{500} e^2_{ch_4,ext}(\tau)\,d\tau$, right. Comparison of configurations I.12 and I.16 for different values of the prediction horizon T_p.

In Figure 9.23 all results obtained for the constant setpoint are visualized. Both for the ideal and real world model together. It can be seen that for some configurations the achieved results for both models are quite different but for some they are almost the same. Here the focus is on the configurations leading to different results.

The configuration I.12 (SMS-EMOA) with $T_p = 10$ d yields very bad results. This is especially true for the integral over the squared control error $e_{ch_4,ext}$ while controlling the real world model (see most right plot in Figure 9.23). The reason for this huge control error is that at the end of the simulated control duration at day 170 the control for some reason leaves the setpoint. After 500 days this rather small deviation from the setpoint has summed up to this large value. The reason why the control leaves the setpoint at that time is that due to the badly chosen feed ammonia increases so that it affects the fitness value negatively. This lets the control change its feed leading to the setpoint deviation which is kept until the end after the control is switched off at day 170.

Using SMS-EMOA with $T_p = 25$ d different results for the substrate feed are obtained. This leads to the totally different results for the fitness value and steady-state stage cost. The same is true for configuration I.16 (CMA-ES) with $T_p = 25$ d. But here, this only affects the one-dimensional steady-state stage cost.

One can say that the smaller the prediction horizon the larger are the deviations of the real world simulation results from their ideal counterparts. Below a prediction horizon

of $T_\mathrm{p} = 100$ d no satisfying results are obtained. But, for $T_\mathrm{p} = 100$ d the simulation results for the real world model are almost the same as for the ideal model.

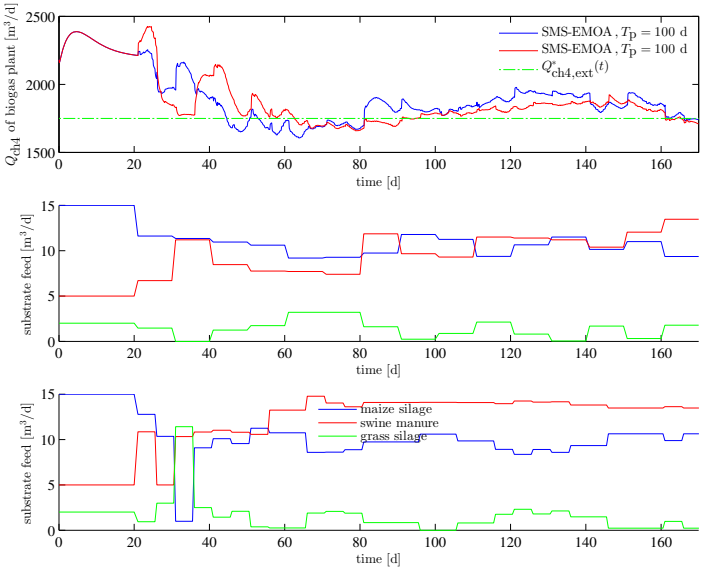

Figure 9.24: Setpoint control for real world model: Comparison of two tests using configuration I.12 with $T_\mathrm{p} = 100$ d, $T_\mathrm{c} = 10$ d and $T_\mathrm{c} = 5$ d, respectively. Top: Methane production of the biogas plant with setpoint $Q^*_{\mathrm{ch_4,ext}}(t)$. In blue the CH_4 production of the control with $T_\mathrm{c} = 10$ d and in red the one with $T_\mathrm{c} = 5$ d is visualized. Middle: Substrate feed of the control with $T_\mathrm{c} = 10$ d. Bottom: Substrate feed of the control with $T_\mathrm{c} = 5$ d.

In a last test the value for the control horizon is set to $T_\mathrm{c} = 5$ d instead of the value of $T_\mathrm{c} = 10$ d used in the previous tests. The test results for configuration I.12 with $T_\mathrm{p} = 100$ d for both control horizon values can be seen in Figure 9.24. It can be observed that the RTO with $T_\mathrm{c} = 5$ d tracks the given setpoint $Q^*_{\mathrm{ch_4,ext}}(t)$ a little bit more accurately. In the tests the process control is switched off, to only see the performance of the NMPC. That the NMPC with $T_\mathrm{c} = 5$ d has a better tracking performance could be expected, because the offline analysis of the substrate feeds are done in a five day interval (see Figure 9.4) so that the expected methane production can be predicted more accurately. However, if the process control is switched on it in general is able to adapt the feed so that the difference in results for both controls will be marginal. Because feed analysis is expensive the usage of a higher rate of analyses and a shorter control horizon in some cases might not be economically reasonable.

9.3.6 Experiment IV: State Estimator

In the last experiment which is presented in this section those tests yielding the best results in the above three experiments (Sections 9.3.3 - 9.3.5) are repeated. The only

difference is that this time the state estimator developed in Chapter 8 is used instead of the ideal state estimator used before. Thus, the control loop sketched in Figure 9.1 is utilized instead of the one in Figure 9.2 which is used in the other experiments. In this section is studied whether the corresponding tests yield approximately the same results. In contrast to the ideal state estimator the real estimator does not assume that the complete state vector of the ADM1 can be measured. Instead, the estimates of the real estimator are only based on a few measured process values (for details see Chapter 8). Therefore, if in this experiment satisfying results are obtained the control in principle will be ready to be used in practice.
As time and resources are limited not all tests are repeated. Only those tests are repeated that achieved best results in the previous experiments. They are:

- Experiment I: Configuration I.16: CMA-ES, $T_\mathrm{p} = 150$ d.
- Experiment II: Configuration I.16: CMA-ES, $T_\mathrm{p} = 150$ d, soft control.
- Experiment III: Configuration I.16: CMA-ES, $T_\mathrm{p} = 75$ d for 1st setpoint and CMA-ES, $T_\mathrm{p} = 100$ d for 2nd setpoint.

Similar results were already published in Gaida et al. (2012a) in the course of this thesis.

9.3.6.1 Setup

As the used state estimator just returns a class label for each state vector component $\hat{x}_{i_\mathrm{x}}$ based on the input variables, the real value for each component is in between a lower and upper boundary defined by the previously in Section 8.2 applied splitting of the state vector components into $C = 10$ classes. Remember that the state estimation problem is solved as a classification task (see Section 4.1). Instead of using the center values in between these lower and upper boundaries (named $\mathbf{lb}_\mathrm{x} \in \mathbb{R}^{n_\mathrm{x}}$ and $\mathbf{ub}_\mathrm{x} \in \mathbb{R}^{n_\mathrm{x}}$, respectively) that state vector as current state estimate is used, whose maximum norm of its derivative is minimal. Thus, the current state estimate $\hat{\boldsymbol{x}}_k$ is defined as:

$$\hat{\boldsymbol{x}}_k := \arg \min_{\mathbf{lb}_\mathrm{x} \leq \boldsymbol{x} \leq \mathbf{ub}_\mathrm{x}} \left| \boldsymbol{f}\left(\boldsymbol{x}, {}^{o}\boldsymbol{u}_k^*\left(t_k - \delta\right)\right) \right|_\infty \tag{9.17}$$

In eq. (9.17) is searched for a steady-state solution by varying the states $\boldsymbol{x}$ inside the allowed range $\mathbf{lb}_\mathrm{x} \leq \boldsymbol{x} \leq \mathbf{ub}_\mathrm{x}$. Thus, using this definition the chance should be increased that simulations of the RTO starting at $\hat{\boldsymbol{x}}_k$ converge to a steady-state solution respectively converge at all. This optimization problem is solved using CMA-ES with a population size of 25 and four generations.
For the setup details to each experiment please consult Section 9.3.3 to Section 9.3.5.

9.3.6.2 Results: Experiment I

In Figure 9.25 optimization results for the tests I.A16 until I.D16 are shown once using the ideal and once using the real state estimator. As with CMA-ES a single-objective

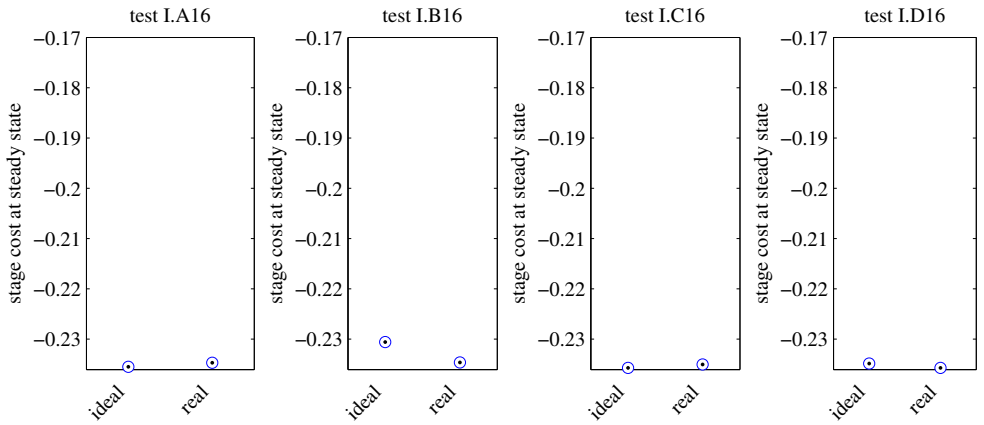

Figure 9.25: Experiment I: Test results of configurations I.A16 - I.D16 for the control using the ideal vs. the real state estimator. As in configuration I.16 the method CMA-ES is used only the one-dimensional steady-state stage cost F_{1D} at day 750 is visualized. All four tests I.A16 - I.D16 using the ideal state estimator are repeated once.

optimization method is used only the one-dimensional steady-state stage cost F_{1D} is shown. It can be seen that the obtained results for the one-dimensional steady-state stage cost are very similar and almost independent of the choice of the estimator. Therefore, it can be concluded that using the real state estimator steady states are found that are as good as the ones found with the ideal estimator.

9.3.6.3 Results: Experiment II

In Figure 9.26 simulation results for the best configuration from experiment II are presented. This is configuration I.16 as the soft implementation. In the top row the simulated methane production and the given methane setpoint $Q^*_{\mathrm{ch}_4,\mathrm{ext}}(t)$ are shown. In the middle row the fed substrates of the control with the ideal estimator and in the bottom row the ones proposed by the control with the real estimator are visualized. It can be seen that the results using the real state estimator are very bad. The reason is that the control has trouble to track the given setpoint. As the initial state estimate is not very accurate only at the end of the prediction horizon the setpoint might be achieved if the correct feed is chosen. Therefore, actually good feeds are evaluated badly. Furthermore, the state estimator is only calibrated for an amount of grass silage between 0 $\frac{\mathrm{m}^3}{\mathrm{d}}$ and 5 $\frac{\mathrm{m}^3}{\mathrm{d}}$, see Table 8.2. So, in case the control would suffice to feed high amounts of grass silage as it would be required, the state estimates might be unpredictably inaccurate. At least the feed at the end of the test is very close to the optimal one, where the test was started from.
To make setpoint tracking work, the way how the control error is included in the objective function must be revised. Once the setpoint is lost, in the current implementation

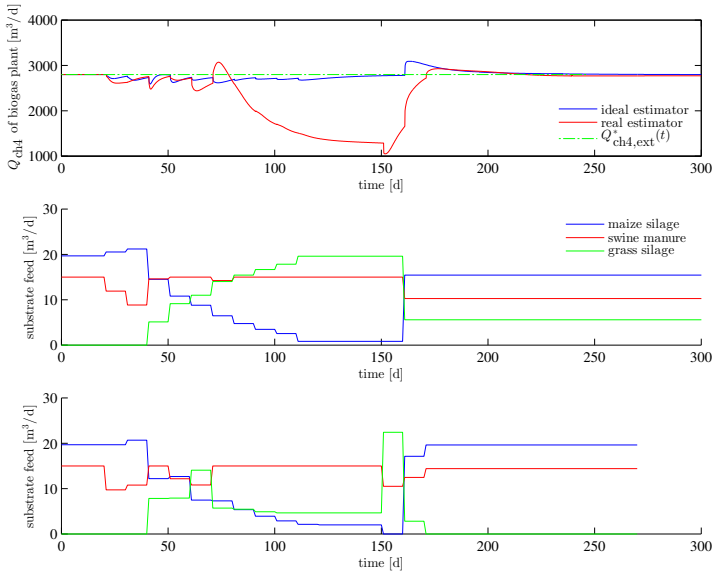

Figure 9.26: Experiment II: Comparison of controls with ideal vs. real state estimator for "soft" control configuration I.16 and $T_\mathrm{p} = 150$ d. Top: Methane production of the biogas plant and methane setpoint $Q^*_{\mathrm{ch_4,ext}}(t)$. Middle: Substrate feed of the control with ideal state estimator. Bottom: Substrate feed of the control with real state estimator. The test using the real state estimator was terminated after 270 days because of exhausted resources on the computer.

a very large and a small control error are evaluated the same. This leads to very large deviations from the setpoint as it can be seen in Figure 9.26.

Table 9.4: Results of control using ideal and real state estimator for configuration I.16 with $T_\mathrm{p} = 150$ d in experiment II.

state estimator	$J_{1\mathrm{D}}$ (300 d)	$F_{1\mathrm{D}}$ (500 d)	$10^{-6} \cdot \int_0^{500} e^2_{\mathrm{ch_4,ext}}(\tau)\,\mathrm{d}\tau$
ideal	-0.015	-0.219	2.31
real	0.202	-0.218	136.71

Table 9.4 compares the obtained results visualized in Figure 9.26 by means of three performance measures. Based on these it can also be easily observed that the performance of the test using the real state estimator is far worse than the one using the ideal state estimator.

9.3.6.4 Results: Experiment III

In Figure 9.27 the achieved control trajectories for the 1st setpoint using the ideal model are shown. The figure compares the results obtained with the real and ideal

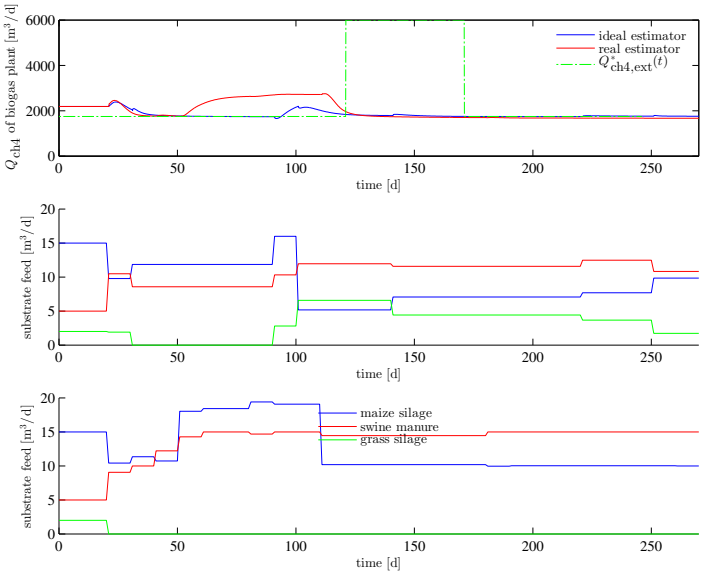

Figure 9.27: Experiment III: Setpoint control for ideal model and 1st setpoint: Comparison of two tests with ideal and with real state estimator using configuration I.16 with $T_p = 75$ d. Top: Methane production of the biogas plant with setpoint $Q^*_{ch_4,ext}(t)$. Middle: Substrate feed of the control with ideal state estimator. Bottom: Substrate feed of the control with real state estimator.

state estimator. Although there is a small difference between both simulation results, using the real state estimator the setpoint is tracked accurately enough.

In Figure 9.28 the control results for the 2nd setpoint at the ideal model are shown. The trajectories obtained using the ideal and real state estimator are compared. It can be seen that the control using the real state estimator does not track the setpoint as accurately as the other, but the control error is quite small. The difference in the obtained feed mixtures is also only marginal.

Figure 9.29 visualizes the results obtained for the 2nd setpoint at the real-world model. Due to the noisy model the setpoint is not tracked exactly. As the simulations starting at the real state estimate, at the start of the simulations are very inaccurate the predicted biogas production of the RTO at the start is very unreliable. Therefore, using the real state estimator the process control is not used, because the setpoint trajectory generated by the RTO would be unpredictably inaccurate.

In Figure 9.30 simulation results for the setpoint experiment using the real and ideal state estimator are shown. In the two plots on the left side of the figure results of the first setpoint (see Figure 9.27) are visualized. The remaining three plots on the right side present the results for the second setpoint (see Figure 9.28).

For the 1st setpoint the results using the real state estimator are not that good as

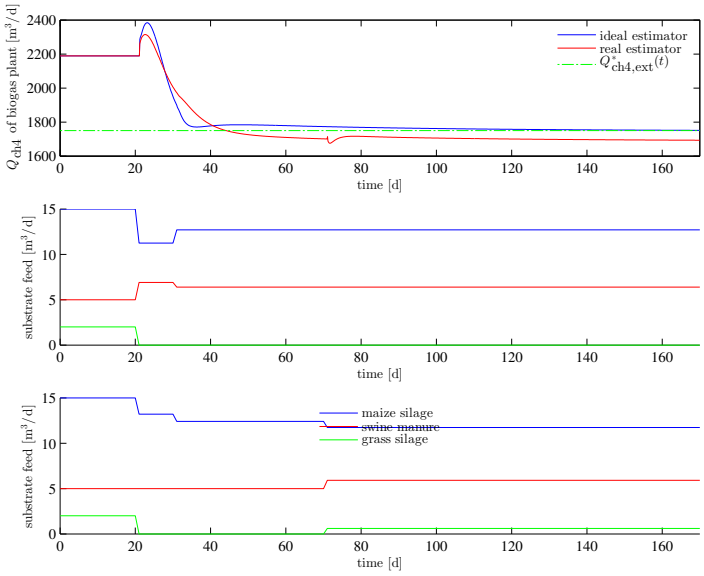

Figure 9.28: Experiment III: Setpoint control for ideal model and 2nd setpoint: Comparison of two tests with ideal and with real state estimator using configuration I.16 with $T_\mathrm{p} = 100$ d. Top: Methane production of the biogas plant with setpoint $Q^*_{\mathrm{ch}_4,\mathrm{ext}}(t)$. Middle: Substrate feed of the control with ideal state estimator. Bottom: Substrate feed of the control with real state estimator.

the ones using the ideal state estimator. The reason is that the setpoint is not tracked accurately which increases both fitness and stage cost values. For the 2nd setpoint the deterioration of both values is introduced because the methane content of the produced biogas is below 50 %. This is a hard boundary defined in the objective function.

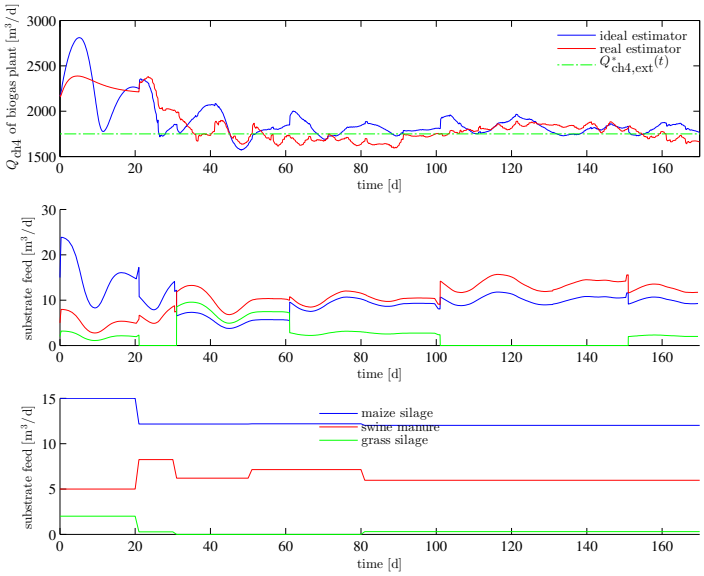

Figure 9.29: Experiment III: Setpoint control for real-world model and 2nd setpoint: Comparison of two tests with ideal and with real state estimator using configuration I.16 with $T_\mathrm{p} = 100$ d. Top: Methane production of the biogas plant with setpoint $Q^*_{\mathrm{ch}_4,\mathrm{ext}}(t)$. Middle: Substrate feed of the control with ideal state estimator. Bottom: Substrate feed of the control with real state estimator.

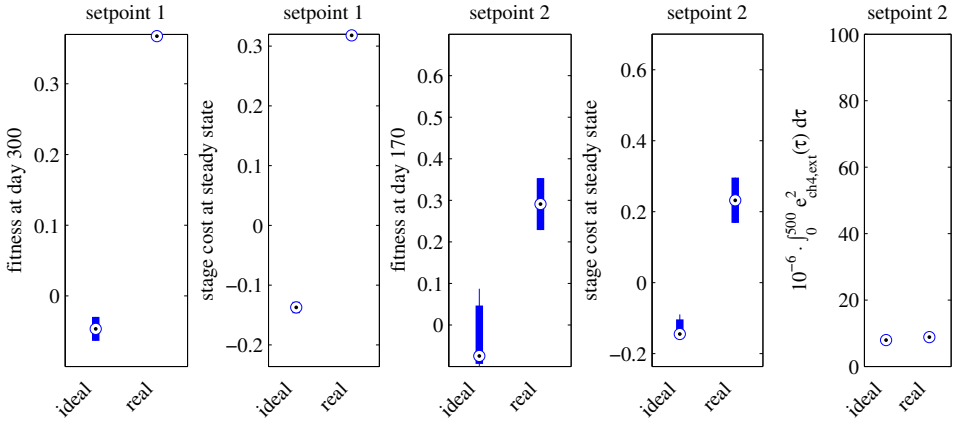

Figure 9.30: Setpoint control for ideal and real-world model using real and ideal state estimator. 1st setpoint: Results for fitness at the end of the simulated control duration ($J_{1\mathrm{D}}$ (300 d), left), one-dimensional steady-state stage cost ($F_{1\mathrm{D}}$ (500 d), middle left). 2nd setpoint: Results for fitness at the end of the simulated control duration ($J_{1\mathrm{D}}$ (300 d), middle), one-dimensional steady-state stage cost ($F_{1\mathrm{D}}$ (500 d), middle right) and the integral of the squared control error over 500 days: $10^{-6} \cdot \int_0^{500} e^2_{\mathrm{ch}_4,\mathrm{ext}}(\tau)\, \mathrm{d}\tau$, right.

9.4 Summary and Discussion

The real-time optimization scheme in principle is able to find the optimal substrate feed with respect to a multi-objective objective function. The tests in experiment I revealed that the basin of attraction of the control is quite large and the optimal feed is kept once it is found. Under changing availability of substrates the predicting behavior of the control helps to change the substrate feed smoothly and to avoid a temporary deterioration of performance (see experiment II). As setpoint control a minimal prediction horizon of $T_\mathrm{p} = 100$ d is needed as was observed in experiment III. This can also be said in general. A prediction horizon between 100 and 200 days can be suggested in general for all performed experiments.

Using the real instead of the ideal state estimator introduces some difficulties. Although the steady-state results are almost the same more dynamic scenarios such as changing the substrate feed or a setpoint tracking task are more challenging. With the used state estimator it is not yet possible to change the substrate feed without a loss in plant efficiency. Setpoint tracking is not that accurate but is possible. However, if more measurements are included in the state estimator, improved results will most certainly be observed.

In the following subsections 9.4.1 - 9.4.6 six extensions of the developed RTO control scheme are discussed. They are:

- Providing balancing energy for secondary and tertiary control.
- Parameter estimation and re-calibration of the process model and state estimator.
- Extension of the control scheme by a supervised expert system.
- Use of models to extend the process control.
- Increasing the speed of the RTO scheme.
- Implementation of simulation model and process control in different units.

9.4.1 Providing Balancing Energy for Secondary and Tertiary Control

Since the amendment of the Renewable Energy Sources Act in 2012 biogas plants in Germany may be used to provide balancing energy for secondary and tertiary control. Nowadays, with the high amount of renewable electrical energy production, the energy market is deregulated. In this market the price for electrical energy is volatile and its prediction is very valuable (cf. Che and Wang (2010), Esfahani (2011)). In Figure 9.31 an exemplary curve of block prices for electrical energy taken from the EPEX SPOT market is shown. When a biogas plant is participating in this market it must be able to start up or bring down its energy production within five (secondary) or fifteen minutes (tertiary), respectively[4]. As a biogas plant is a very slow system such fast responses are

[4] http://www.next-kraftwerke.de/wissen/regelenergie
http://www.next-kraftwerke.de/energie-blog/praequalifikation-regelenergiemarkt

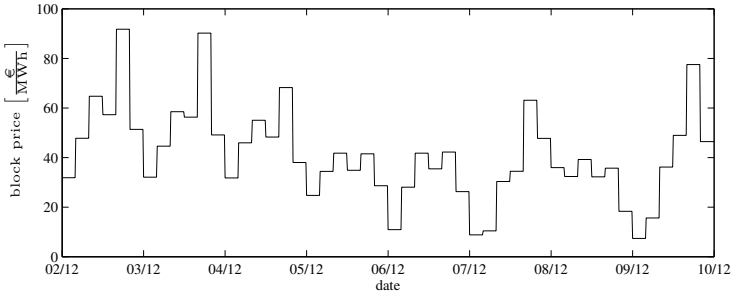

Figure 9.31: Block prices for electrical energy at the EPEX SPOT auction between 02/12/2013 and 09/12/2013.

only possible when the biogas plant has a gas storage unit. Here, an optimal control has the task to always keep the volume in the gas storage half-full so that the biogas plant can provide positive as well as negative balancing energy in the same amount. To predict the gas volume in the storage unit a model-based predictive control can use the predicted biogas production and the requested energy profile over the prediction horizon. To keep the gas storage unit at a minimal installation size a good prediction as well as an accurate setpoint tracking control is needed. As a minimum the gas volume should be able to store the produced biogas for a few hours at maximal biogas production.

As already written in the summary of Chapter 7 a gas storage unit is not yet implemented in the biogas plant model. Therefore, such a setpoint tracking problem unfortunately could not yet be simulated in this thesis.

9.4.2 Parameter Estimation and Re-Calibration of the Process Model and State Estimator

The problem with modeling of biogas plants is that after some time there will be a mismatch between model predictions and real plant behavior. There are numerous reasons that could lead to this situation. Examples are:

- Adaptation of anaerobic bacteria to (inhibiting) conditions in the digester.
- Insufficient calibration of model parameters (that are only locally valid).
- Drift in online measurement devices such as gas analyzer, pH and TS sensor.
- Change of substrate characteristics that are not measured, e.g. inclusion of toxic substances.
- Digester and substrate probes used for calibration are far from representative for the complete digester content or substrate storage.
- Unmodeled processes happening on the biogas plant such as some biochemical processes or process disturbances.

The questions are how to detect whether the model and the process are drifting apart and what is the reason for that. The first question is way easier to answer.
There are at least two methods to detect a deterioration of process model predictions. The first idea is to compare the simulated state vector of the last iteration ${}^{o}\boldsymbol{x}\left(t_{k-1}+\delta\right)$ with the predicted state vector of the current iteration $\hat{\boldsymbol{x}}_k$ on a moving horizon. If the sum of the deviation of both "predictions" ${}^{o}\boldsymbol{x}\left(t_{k-1}+\delta\right)-\hat{\boldsymbol{x}}_k$ over some horizon exceeds an upper boundary a drift between predictions of the process model and the real process behavior is very likely. The only problem of this approach is that both predictions are based on the same model. Therefore, in a worst case scenario, it is possible that a drift maybe remains undetected.

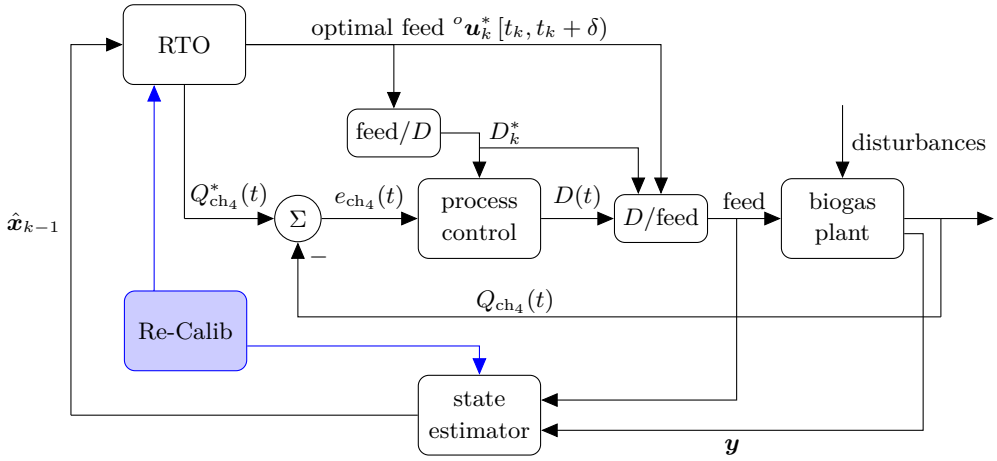

Figure 9.32: Real-Time Substrate Feed Optimization with a Re-Calibration Module. This figure is equal to Figure 9.1 with the only change that here a module to re-calibrate the process model and the state estimator is integrated. The new module is colored in blue.

The second idea is based on the fact that the control error $e_{\mathrm{ch}_4}(t)$ must be minimal and at the same time the optimal feed ${}^{o}\boldsymbol{u}_k^*\left[t_k, t_k+\delta\right)$ and the really applied feed $\boldsymbol{u}_{\mathrm{ctrl}}(t)$ (see eq. (9.6)) will be approximately the same if the model is perfect. The error between both feeds shall be denoted by $\boldsymbol{\Delta u}_{\mathrm{ctrl}}(t) := \boldsymbol{u}_{\mathrm{ctrl}}(t) - {}^{o}\boldsymbol{u}_k^*\left[t_k, t_k+\delta\right)$. By observing the weighted sum of both error terms over a moving window

$$\int_{t_k-N_{\mathrm{ctrl}}\cdot\delta}^{t_k} \boldsymbol{\Delta u}_{\mathrm{ctrl}}^T(\tau)\cdot\boldsymbol{Q}_{\mathrm{ctrl}}\cdot\boldsymbol{\Delta u}_{\mathrm{ctrl}}(\tau)+e_{\mathrm{ch}_4}^2(\tau)\mathrm{d}\tau > \epsilon_{\mathrm{ctrl}}$$

it can be identified whether there is a deviation between model prediction and plant behavior. There, $\boldsymbol{Q}_{\mathrm{ctrl}}$ is a weighting matrix, $\epsilon_{\mathrm{ctrl}} \in \mathbb{R}^+$ is an upper boundary and $N_{\mathrm{ctrl}} \in \mathbb{N}$ defines the length of the moving window.
To answer the second question from above - what is the reason for the deviation of model predictions? - is very difficult. The reason is that there are many possible reasons

for this deviation as is listed above. By regular re-calibration of the online measurement devices their drift can at least be limited so that one item of the list above can be solved. A drift in methane concentration measurement could be detected by a static model calculating the biomethane potential of the substrate feed or by reverse calculation using the produced electrical energy assuming a constant electrical degree of efficiency of the CHPs and a drift free measurement of biogas production.
If, in case of a plant-model mismatch, model parameters should be re-calibrated the question arises whether they can be estimated reliably given available online and offline measurements of the plant. The field dealing with this kind of question is called practical identifiability analysis (Brun et al., 2001, Dochain and Vanrolleghem, 2001, Raue et al., 2009, 2011). To the author's knowledge such a practical identifiability analysis has not yet been performed for the ADM1. As on full-scale biogas plants there are only a few online or frequently measured values, practical identifiability of most ADM1 parameters will be rather difficult. The reason is also that most full-scale biogas plants are operated at steady state and therefore kinetic parameters cannot be determined. With a shift of biogas plant operation to demand-oriented operation this might change in the future.
If a model mismatch is detected a re-calibration module could be implemented as is sketched in Figure 9.32.

9.4.3 Extension of the Control Scheme by a Supervised Expert System

Due to the complexity of the anaerobic digestion process also the most detailed model is always only a very scarce approximation of reality. As a failure in biogas plant operation can be very expensive one should not trust the RTO suggested feeds blindly. As optimal operation often also means risky operation in special situations the suggested feeds must be used with care. Therefore, a scheme as sketched in Figure 9.33 is suggested.

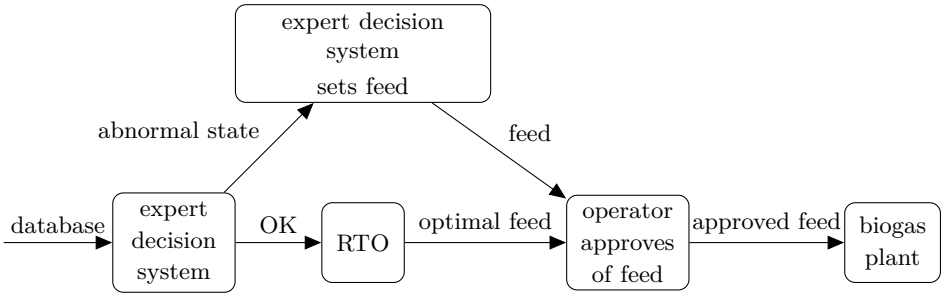

Figure 9.33: Expert decision system and operator are important parts of the closed-loop feed control.

In Figure 9.33 an expert system superimposes the RTO scheme and in special situations may overrule it. The expert system could be a rule-based system that analyses in which

state the biogas plant is in and based on that it decides whether the state is normal or abnormal. If the state is normal the RTO may propose its optimal substrate feed. If the state is abnormal then the expert system suggests a feed that is maybe more safe. The rules in the expert system could be defined by the biogas plant's operator using his valuable expert knowledge. The state detection of the expert system is based on the available data in the database and explicitly also can use measurements that can not be used in a mechanistic simulation model yet. This means that the state also may contain variables that can not be modeled yet. The final decision of the expert system might be implemented using fuzzy logic.
No matter which system suggests the feed it is always recommendable that the operator always has to approve (release) the feed before it is fed to the biogas plant, see Fig. 9.33.

9.4.4 Use of Models to Extend the Process Control

The process control Antonelli et al. (2003) that is used in the RTO control scheme above is not model-based. The literature review in Chapter 6 revealed that many process controls do exist that could be used instead of Antonelli et al. (2003). In the following some ideas are collected that could be worth investigating to improve the process control.
To use a MPC as process control using the linearized ADM1 would be a straight forward extension of the RTO scheme. As the state of the ADM1 is already estimated by the state estimation method the state estimate for the MPC comes for free. As nowadays it is no problem any more to solve a convex optimization problem online, to develop such a process control could be worth a try. The interested reader is referred to the following literature for a quick start: Kauder et al. (2007), Benhalla et al. (2010), Smets et al. (2003).
Instead of using the linearized ADM1 one could also use the singular thresholding method to create a linear model (Qin and Badgwell, 2003).

9.4.5 Increasing the Speed of the RTO Scheme

The time to solve the nonlinear optimization problem at each control sampling time is quite long and needs a lot of resources. Therefore, to shorten this time is of great interest. The time consuming part in the optimization problem is the evaluation of the objective function $\boldsymbol{J}$ because it triggers a simulation of the biogas plant model. By using approximations of the complex model these times can severely be reduced. This approach is also followed by the method SMS-EGO (see Section 3.2) using a DACE model. This DACE model is learned on the fly using simulation results of the expensive model. An extension of this idea would be to use the methods of Co-Kriging (Forrester

et al., 2007). There, also simpler models can be used to train the DACE model and by that improve the quality of the resulting DACE model.
Static models are examples of such simpler models. Two ideas are presented in the following.
The first idea is to use a state dependent static model. Based on the current state and constant substrate feed of the plant it predicts its steady state solution. As noted in subsection 9.3.3.2 above most of the time the steady state of a biogas plant does not depend on its initial state but only on the substrate feed. Therefore, this model most of the time would be a usual static one and only for some special regions of the state space it would be state dependent. Such a model could be created as a "black-box" model which is trained beforehand by simulations with the complex simulation model.
The second idea would be to use a mechanistic static model. Based on the biomethane potential (Angelidaki et al., 2009) of a substrate its potential for energy production can be estimated. Furthermore, given the purchasing cost of a substrate an economic gain can be calculated. Using this, the economic gain of a substrate mixture can be obtained. This is a very gross approximation of the complex model but it is a very simple and fast one. This approach is currently investigated by my colleague Martin Zaefferer at Cologne University of Applied Sciences.

9.4.6 Implementation of Simulation Model and Process Control in Different Units

Using the biogas plant model and the process control in the same Simulink® model causes numerical difficulties for the ODE solver to simulate the model. Therefore, separating both components in two different Simulink® models might be an option. Communication and synchronization of both might be possible using OPC (formerly: OLE for process control[5]).

[5] http://www.opcconnect.com/